NOTICE

The quality of this microform is heavily dependent upon the quality of the original thesis submitted for microfilming. Every effort has been made to ensure the highest quality of reproduction possible.

If pages are missing, contact the university which granted the degree.

Some pages may have indistinct print especially if the original pages were typed with a poor typewriter ribbon or if the university sent us an inferior photocopy.

Reproduction in full or in part of this microform is governed by the Canadian Copyright Act, R.S.C. 1970, c. C-30, and subsequent amendments.

AVIS

La qualité de cette microforme dépend grandement de la qualité de la thèse soumise au microfilmage. Nous avons tout fait pour assurer une qualité supérieure de reproduction.

S'il manque des pages, veuillez communiquer avec l'université qui a conféré le grade.

La qualité d'impression de certaines pages peut laisser à désirer, surtout si les pages originales ont été dactylographiées à l'aide d'un ruban usé ou si l'université nous a fait parvenir une photocopie de qualité inférieure.

La reproduction, même partielle, de cette microforme est soumise à la Loi canadienne sur le droit d'auteur, SRC 1970, c. C-30, et ses amendements subséquents.

ISBN 0-315-56050-9

Tailings Dam Failure due to Liquefaction of the Retained Deposit

Ignazio Bozzo

A Thesis

in

The Department

of

Civil Engineering

Presented in Partial Fulfillment of the Requirements
for the Degree of Master of Engineering at
Concordia University
Montréal, Québec, Canada

March 1990

ABSTRACT

Tailings Dam Failure due to Liquefaction
of the Retained Deposit

Ignazio Bozzo

In recent decades, failures of tailings dams due to earthquakes have resulted in the loss of many human lives and extensive financial and environmental damage. The main factor being the liquefaction and flow of the retained deposit. Furthermore, in a number of occasions, it has been noted that failure of the tailings dam occurs well after the succession of earthquake activities.

The tailings dam comprises a family of dams, composed of a starter dam and a number of secondary dams, which retain very loosely deposited fine-grained and usually saturated material. In the event of a severe seismic shock, the retained deposit tends to liquefy, leading to the development of high pore water pressure in the body of dams and consequently to a belated failure of the system. This mode of failure was diagnosed by Professor K. Ishihara during a lecture given at Concordia University in 1985.

This thesis describes a method of analysis of the development of pore water pressure within an upstream type of tailings dam. Using a finite element method computer program, the phreatic surface and the corresponding distribution of pore water pressure in the tailings dam, during the state prior to the earthquake and the state after the liquefaction of the retained deposit, are determined. The results of the solution for both cases are compared and, the stability of the tailings dam, for the latter state, is analyzed.

This study shows that for the post-liquefaction case, the relative level of the phreatic surface increases within the tailing dam and the corresponding increase in the magnitude of the pore water pressure distribution may easily induce instability and cause failure of the system as a whole.

ACKNOWLEDGEMENTS

The author wishes to express his sincere gratitude to Dr. H.B. Poorooshasb for his constructive guidance, encouragement and fruitful suggestions which have made the successful completion of this thesis possible.

The financial assistance of the Natural Sciences and Engineering Research Council of Canada is greatly appreciated.

Finally, an obligation of gratitude is extended towards my beloved family for their unfailing moral support and understanding. Also, very special thanks are due to Julia for her patience and encouragement and, for always being there.

TABLE OF CONTENTS

Page

LIST OF FIGURES

LIST OF TABLES

LIST OF SYMBOLS

ENGLISH

c'	effective cohesion
D	height of water on upstream side of dam
d	height of water on downstream side of dam
e	void ratio
f	prescribed constraint for the hydrostatic head
G	specific gravity (solids)
H	elevation of phreatic surface at a given point
h	total hydrostatic head or potential
h_1, h_2, h_3	fluid head at three nodes in one element
k	coefficient of permeability in both the x and y directions
P_1, P_2, P_3	parameters expressing h_1, h_2, h_3
P^j	a 3x3 coefficient matrix
p_1, p_2	constants in the functional U
Q	externally applied fluid flux
q_n	prescribed fluid flux input
R	region of the medium
S	degree of saturation
$S_1 + S_2$	entire boundary of the region R
t	time
U	a functional of the variational principle
U_j	integral over a single element
u	pore water pressure
y	elevation head

GREEK

γ_d	dry density
$\gamma_{sat\ (slimes)}$	saturated density of the slimes
$\gamma'_{sat\ (sands)}$	effective saturated density of sands
$\gamma'_{sat\ (slimes)}$	effective saturated density of slimes
γ_t	total unit weight (total density)
γ_w	unit weight of water
Δ	determinant of system of linear equations
η	porosity of the medium
σ	total normal stress
σ'	effective normal stress
τ	shearing resistance or strength
$\tau_{available}$	shearing strength available (mobilized) on selected plane(s)
$\tau_{applied}$	shearing force applied on selected plane(s)
ϕ'	effective angle of shearing resistance or friction

SPECIAL

$^\circ$	degrees
$\int$	integral
Σ	summation
/	per
∇	water level

CHAPTER 1

INTRODUCTION

In this chapter, is included a brief history of the belated failure phenomenon of tailings dams associated with the liquefaction of the retained deposit, as may occur due to a severe earthquake. Also, presented at the end of this chapter are the objectives and contents of this thesis.

1.1 Foreword

Throughout the mining industry, tailings are the residual waste product after the extraction of valuable minerals. Tailings deposits, commonly developed for the placing of the waste material, consist of two major components. The first component is a fairly permeable family of dams (i.e., tailings dam), composed of a starter dam and a number of secondary dams. The secondary dams are constructed using the coarser fraction of the tailings, as the level of the impounded material increases. The second component is the body of the retained material, consisting of very loose, saturated and relatively finer tailings (i.e., slimes).

In a number of occasions, it has been noted that when the site is subjected to a severe earthquake, the tailings dam does not fail during the period of strong ground motion, rather it fails at a later date (for example, after a period of 24 hours). This mode of failure of tailings dams has received some attention in research but, much more work is needed.

Whitman et al. (1985) maintain that this belated failure is due to the development of negative pore water pressure in the body of the tailings dam during the earthquake (which increases its factor of safety during the earthquake) and the subsequent redistribution of pore water pressure, after the initial phase of pore water pressure decrease. Although some

testing in centrifuges has, in fact, demonstrated the possibility of this happening, the results are not conclusive.

The present writer believes that another mechanism is likely to be the cause of this belated failure phenomenon. According to this mechanism, during the earthquake, the impounded material liquefies and this creates very high stresses behind the family of dams system The subsequent increase in pore water pressure redistributes the regime of pore water pressure within the body of the dams and, in fact, can lead to very high pore water pressures. Accordingly, the level of the phreatic surface increases and this is believed to be the cause of failure (Ishihara, 1984). Since the development of this excess pore water pressure is a function of time, the failure takes place well after the succession of earthquake activities (Poorooshasb and Ishihara, 1989).

1.2 Objectives of this Study

The objectives of this research are the following:

1. Describe a method of analysis for the development of pore water pressure within an upstream construction type of tailings dam during the states prior to and after the complete liquefaction of the retained deposit, as may be caused by a severe earthquake.

2. Solve and analyze the phreatic surface solutions and the corresponding pore water pressure distributions in the body of the tailings dam for the pre-earthquake case and the post-liquefaction case. A comparison of the results obtained for the two cases is carried out at various points and the findings are presented.

3. The stability of the tailings dam during the state after the complete liquefaction of the retained deposit (i.e., post-liquefaction case) is analyzed. A simple static stability analysis of the tailings dam is conducted by selecting a number of critical planes within the tailings dam and determining the factor of safety for each plane selected.

In order to accomplish the second objective, a computer program is written for linear triangular finite elements analysis, verified by ensuring the correctness of final results

with predetermined solutions, and used to obtain the solutions for the two cases analyzed in this study.

1.3 Organization of the Thesis

In Chapter 1, a brief historical background of the related failure phenomenon of tailings dams due to liquefaction of the retained deposit, as may be caused by a severe earthquake, is presented and the objectives of this thesis are reviewed.

A general description of tailings dams, properties of tailings and the concept of liquefaction is given in Chapter 2. In addition, some seismic failure cases of tailings dams are discussed, including details on two of the better documented earthquake-induced tailings dam failure incidents.

The governing equations, assumptions and the finite element formulation of the problem are described in Chapter 3. A description of the computer program written for this study together with its verification are also contained.

In Chapter 4 are determined the phreatic surfaces in the body of an upstream construction type of tailings dam for both the pre-earthquake and post-liquefaction conditions of the tailings deposit. The pore water pressure distributions in the body of the tailings dam, for both cases, are determined and presented.

In Chapter 5, the increase in elevation of the phreatic surface and the pore water pressure increase for various points within the tailings dam are compared for the two cases analyzed. Also, a simple static stability analysis of the tailings dam is carried out for the post-liquefaction case. Finally, the research results, conclusions and suggestions for future work on this subject are presented in Chapter 6.

CHAPTER 2

TAILINGS DAMS AND SEISMIC FAILURE CASES

2.1 Tailings Dams

Tailings dams differ from conventional water storage earth dams in that the bulk of material stored behind the family of dams, i.e., the starter dam and secondary dams, is soft, loose and relatively impervious tailings rather than water. In addition, most of the tailings dams construction is carried out by the mining operators, as part of the tailings disposal operation, with the dam being raised as required to stay ahead of the rising tailings pond. A comparison between the water storage earth dam and the upstream type of a tailings dam is presented in Fig. 2.1.

Tailings dams are commonly used to develop tailing ponds for the storage of the waste products generated by the mine and milling operations. The recent trend towards the mining of very low grade ores has resulted in the need of extremely large tailings dams, often scores of meters in height and retaining millions, or even billions of tons of tailings in slurry form.

Tailings dams are, therefore, structures that involve public concern. Of main importance is the structural stability of the dam and the possible release, if failure occurred, of a very large volume of water and/or semi-fluid tailings. Such an event would not only cause extensive downstream pollution, but would also pose a serious threat to life and property. It is for these reasons that the disposal of tailings is commonly identified as the single most important source of environmental impact for many projects.

2.1.1 Construction Methods

The three methods currently in use for the construction of tailings dams are the upstream method, downstream method and the centerline method (Vick, 1983).

For the upstream method, a sufficiently pervious starter (primary) dam is initially constructed at the downstream toe. Tailings are then discharged from the top of the starter dam using spigots or cyclones (a description of each is included further on in this chapter) to develop the first of several secondary dams composed of their coarser fraction. The

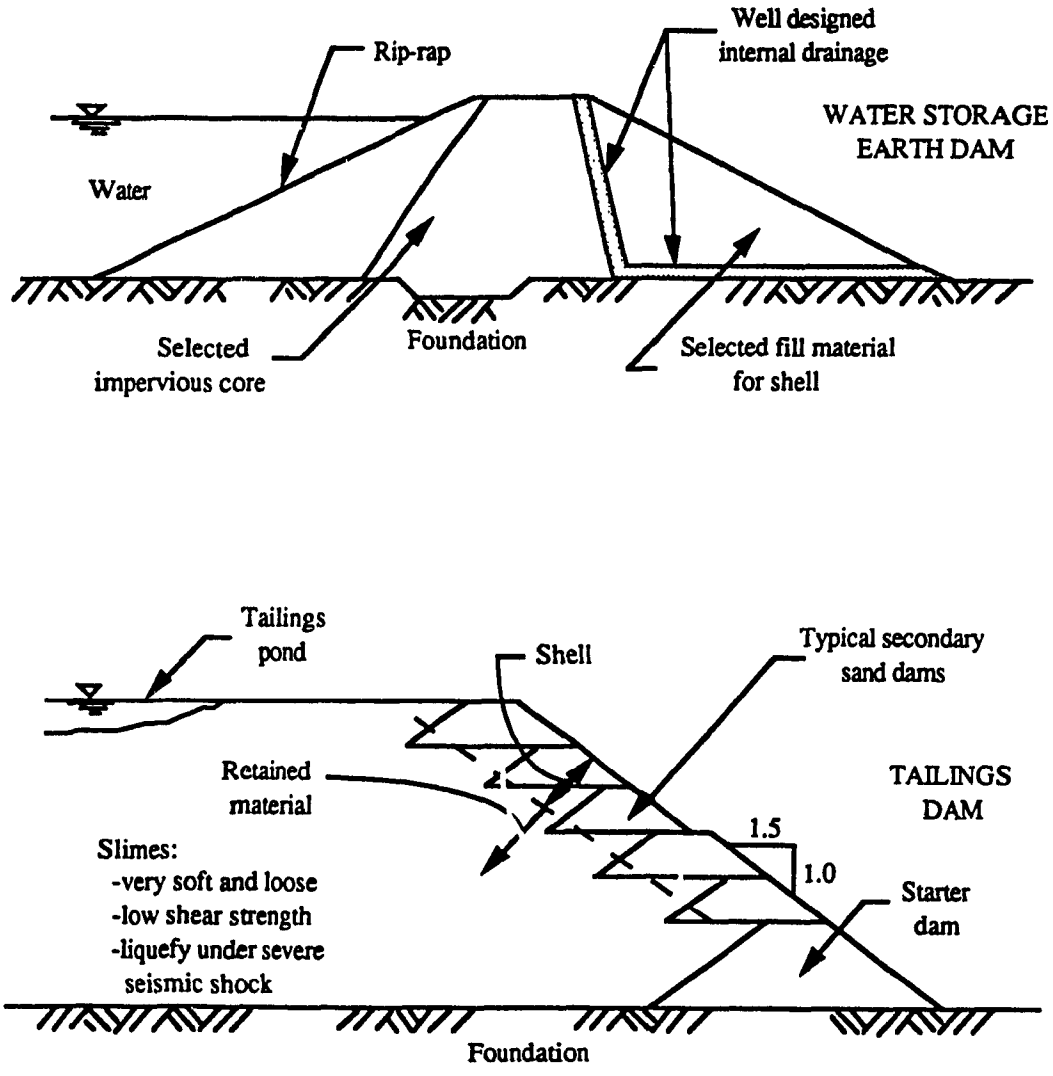

Figure 2.1 Comparison Between Water Storage Earth Dam and Upstream Type of Tailings Dam (Jeyapalan, 1980 and Klohn, 1981).

centerline of the embankment is shifted upstream towards the pond area as the height of the dam increases. That is, the downstream toe of each new secondary dam is supported on the top of the previously built secondary dam whilst the majority of the upstream portion of the new secondary dam is placed over the finer tailings, as shown in Fig. 2.1.

In the downstream method of construction, internal drainage is provided within the relatively impervious body of the dam, i.e, starter dam and secondary dams, and the centerline of the top of the dam shifts downstream as the dam is raised. The centerline construction method is a variation of the downstream method whereby the crest of the dam is maintained at the same horizontal position as the height of the dam is increased. Refer to Fig. 2.2 below.

In both the downstream and centerline methods, the major part of each of the secondary dams is not underlain by the previously deposited tailings, as is the case with the

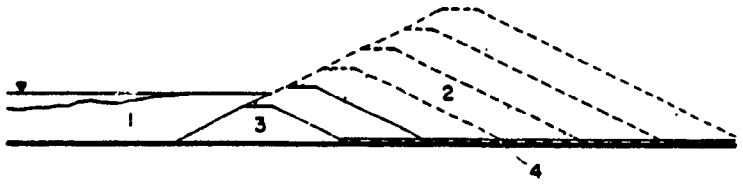

Downstream Method

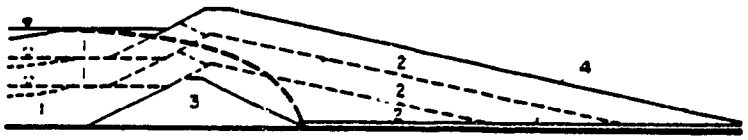

Centerline Method

(1) Slimes.
(2) Sands.
(3) Starter dam.
(4) Drain.

Figure 2.2 Downstream and Centerline Methods of Tailings Dam Construction (Finn, 1981).

upstream construction method. These more stable family of dams are achieved by spreading and compacting additional coarse tailings on the top, downstream slope and/or upstream shoulder of the immediate lower secondary dam(s).

2.1.2 Mining Process of Tailings

Common to most ore milling and mining procedures are the initial steps of crushing and grinding. Then, separation and removal of mineral values in the concentrate is usually performed, leaving the remaining barren particles as tailings. These tailings, which consist of ground-up rock, are normally mixed with water to produce a slurry and then transported to the tailings pond.

The grain-size distribution of tailings depends upon the characteristics of the ore and the mill processes used to concentrate and extract the metal values. A wide range of tailings gradation curves exist for various mining operations are shown in Fig. 2.3.

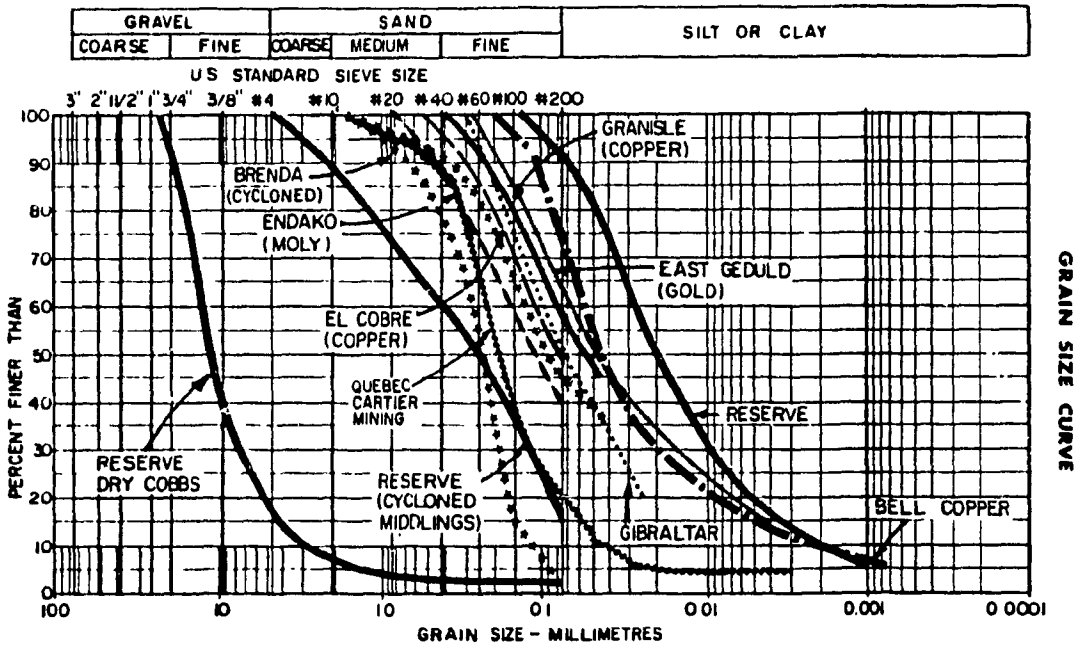

Figure 2.3 Typical Tailings Grain Size Distribution Curves (Klohn, 1981).

Tailings are transported to the disposal area sometimes by gravity flow through open launders but more commonly through pipes at a concentration of approximately 40 percent by weight of solids to liquid. The usage of pumps is usually dictated by the relative elevations of the mill and tailings impoundment, as well as pipe length and head losses.

The deposition of an above-water tailings beach around the inner perimeter of a tailings dam, which is usually mandatory for structural purposes, may be accomplished by either single-point discharge or spigotting (refer to Fig. 2.4 below). Single-point discharge requires that the open end of the tailings discharge pipe be relocated and/or the pipe segments disconnected periodically to form a series of adjacent and overlapping deltas. Spigotting accomplishes the same purpose by discharging tailings slurry through closely spaced spigots in the pipe line (usually about 50-150 ft. apart), which are typically individually valved for control and distribution of discharge.

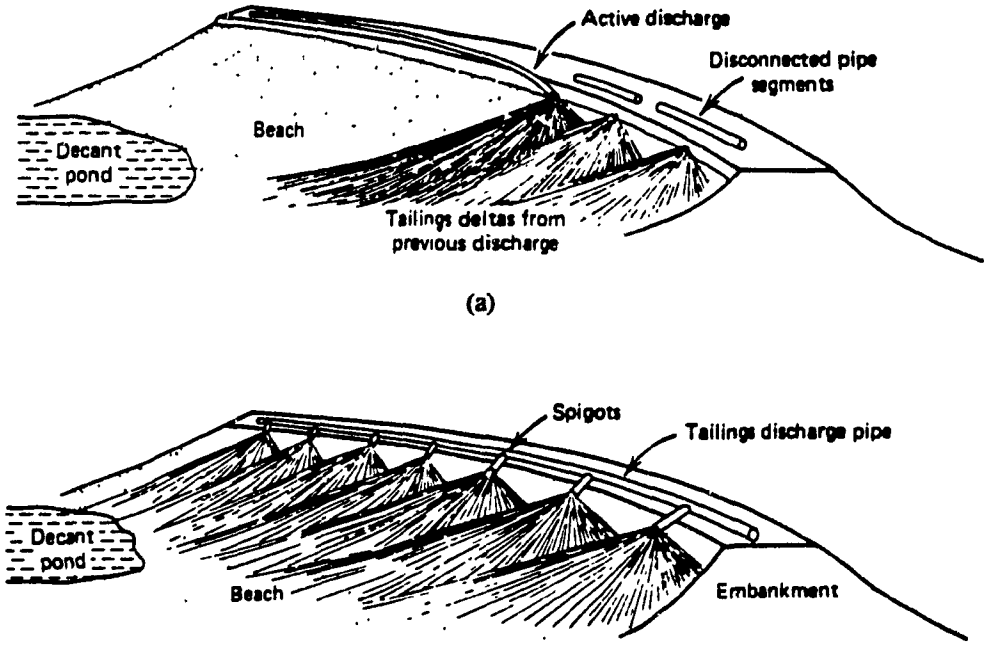

Figure 2.4 Peripheral Discharge Methods (Vick, 1983).
(a) Single-Point Discharge. (b) Spigotting.

When natural soils of suitable type or quantity are unavailable, the relatively cheap method of cycloning tailings to produce sand tailings provides a significant cost advantage in embankment design. That is, since the sand tailings are produced on or very near the embankment itself, the fill hauling costs are drastically reduced or eliminated. Provided the tailings are essentially non-plastic and free of clay minerals, reasonably clean sand tailings can be produced from most tailings having less than 60% passing the No. 200 sieve by using simple devices called cyclones.

Cyclones function on a centrifugal separation principle with no moving parts in which whole tailings slurry is fed under pressure. Separation takes place as the coarser sand fraction spiral downward (underflow) whilst the finer fraction and most of the slurry water rise to the top (overflow), producing slimes.

2.1.3 Engineering Behavior of Tailings

Engineering behavior of tailings includes the depositional characteristics, the in-place and relative densities, and engineering properties (i.e., permeability, compressibility, consolidation, drained shear strength, etc.). However, with regards to the scope of this study, only the in-place densities, the permeability and the drained shear strength of tailings will be discussed.

Of the above-noted engineering properties of tailings, permeability is the most difficult to generalize. Permeability varies as a function of grain size and plasticity, depositional mode, and depth within the deposit (Vick, 1983). Average permeability spans five or more orders of magnitude, from 10^{-2} cm/sec for clean, coarse sand tailings to as low as 10^{-7} cm/sec for well-consolidated slimes. In Table 2.1 are presented typical tailings permeability ranges.

The in-place dry density, which can be expressed in terms of either dry density (γ_d) or void ratio (e), of tailings depends primarily on three factors: specific gravity, type of tailings (sands or slimes), and clay content. Because of variations in all three factors, dry

density spans a wide range, from as low as 14 pcf for clayey phosphate slimes to in excess of 110 pcf for high specific gravity lead-zinc tailings. Typical in-place densities and void ratios for three different types of tailings are shown in Table 2.2.

Their generally loose depositional state notwithstanding, tailings have high drained (effective-stress) shear strength owing primarily to their high degree of particle angularity (Vick, 1983). With rare exceptions, tailings are cohesionless and show a zero effective cohesion intercept, c', in properly performed and interpreted laboratory tests. In the laboratory, the effective friction angle, ϕ', is commonly measured using either consolidated

Table 2.1 Typical Tailings Permeability Ranges (Vick, 1983)

Type	Average Permeability, k (cm/sec)
Clean, coarse, or cycloned sands with less than 15% fines	10^{-2} - 10^{-3}
Peripheral-discharged beach sands with up to 30% fines	10^{-3} - 5×10^{-4}
Nonplastic or low-plasticity slimes	10^{-5} - 5×10^{-7}
High-plasticity slimes	10^{-4} - 10^{-8}

Table 2.2 Typical In-Place Densities and Void Ratios of Tailings (Vick, 1983)

Tailings Type	Specific Gravity	Void Ratio, e	Dry Density, γ_d (pcf)
Copper			
Sands	2.6 - 2.8	0.6 - 0.8	93 - 110
Slimes	2.6 - 2.8	0.9 - 1.4	70 - 90
Lead-zinc			
Slimes	2.6 - 3.0	0.6 - 1.1	80 - 113
Phosphate			
Slimes	2.5 - 2.8	11	14

drained (CD) triaxial or direct shear tests, or consolidated-undrained (CU) triaxial tests with pore pressure measurements. It should be noted that the most important factor influencing ϕ' for tailings is the stress range over which it is measured. Typical values of ϕ' for various materials are shown in Table 2.3.

2.2 Liquefaction of Tailings

Tailings can be classified according to the principles of soil mechanics. As a result of the crushing and grinding operation, the remaining tailings are usually angular, bulky-grained sand, silt and/or clay size particles. These types of particles are known to be susceptible to rapid and large reduction in strength, due to very minor disturbances, if they are deposited in a loose and saturated condition.

Transport of the tailings slurries to the pond, using hydraulic methods, causes the separation of the tailings into sand and slimes. As the slimes settle from the water, they accumulate in loose deposits and the predominantly silt and/or clay sizes may form a meta-stable honeycombed structure, as shown in Fig. 2.5.

Because of this open structure, although slimes have in-place void ratios, *e*,

Table 2.3 Typical Values of Drained Friction Angle (Vick, 1983)

Tailings Type	Drained Friction Angle, ϕ' (deg.)	Effective-Stress Range (psf)
Fine coal refuse	22 - 39	0 - 25,000
Copper		
Sands	33 - 37	0 - 14,000
Slimes	33 - 37	0 - 14,000
Lead-zinc-silver		
Sands	30 - 36	-
Taconite		
Sands	34.5 - 36.5	-

generally in the range of 0.7 to 1.3, slimes of highly plastic clay or unusual composition may have in-place void ratios ranging from about 5 to 11.

According to the principle of effective stress, as formulated by Terzaghi, the strength that a sand can mobilize to resist shearing along an interface, depends on the effective (intergranular) stress on the plane and the effective coefficient of friction. The shearing resistance (strength), τ, may be written as (Finn, 1981):

$$\tau = \sigma' \tan \phi' \tag{2.1}$$

in which σ' is the effective normal stress and ϕ' is the effective angle of shearing resistance (coefficient of friction). In a saturated sand, the effective normal stress, σ', between the grains is the total normal stress, σ, minus the pore water pressure, u, or:

$$\sigma' = \sigma - u \tag{2.2}$$

Thus, the equation for the shear strength becomes:

$$\tau = (\sigma - u) \tan \phi' \tag{2.3}$$

Fine sand and slimes have a rather low permeability and, therefore, excess pore pressure cannot dissipate under rapid dynamic loading conditions, such as those that occur from earthquakes. Since the excess pore pressures for these loose deposits are positive, it is clear from equation (2.3) that as the pore water pressure, u, increases for any reason, the

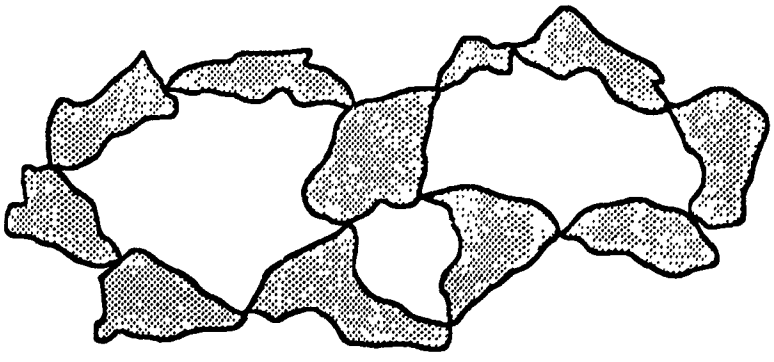

Figure 2.5 Honeycombed Structure of Loosely Deposited Angular Bulky Grained Soils (Lucia et al., 1980).

shear strength, τ, across any plane of failure decreases. When $u = \sigma$, then $\sigma' = 0$ and the material is said to have liquefied.

Liquefaction of a soil may thus be defined as a temporary state in which the structure of the soil is disturbed, causing the loss of point to point contact. This results in the induced shear stresses being transferred to the water in the voids, causing the pore water pressure to rise and the soil behaves like a dense fluid.

Although liquefaction can be caused by changes in static stress conditions, particularly in very loose soils, the more general cause of a structural disturbance leading to liquefaction is dynamic loading, such as can occur during an earthquake.

As shown by Poorooshasb and Ishihara (1989), liquefaction may be induced in certain layers within the body of a tailings deposit and if the structure is not capable of resisting the forces exerted at elevations above the liquefied layer, it may fail. The ease and position with which a liquefied layer can be initiated depends on the physical properties of the material, as well as being a function of the nature and size of the earthquake type excitation.

During the early stage of a severe earthquake, the slimes in the tailings pond, which are usually soft, loose and permanently saturated, will tend to liquefy. Should liquefaction of the slimes occur, an increased horizontal load will be applied on the family of dams (i.e., the starter dam and secondary dams) over and above the normal at-rest pressure to be expected from the pond deposits. This load will give rise to undrained shear stresses within the dam that in turn will cause the pore water pressure to rise. Naturally, according to equation (2.3), this increase in the pore water pressure will reduce the shear strength of the slimes, which will then consequently produce a weakening effect on the dam.

Although common to tailings dams, the above liquefaction phenomenon does not occur in conventional water dams in the sense that the water retained has no shear strength and thus no increased horizontal loads can occur on the dam except for the dynamic effects.

2.3 Seismic Failure Cases

Failures of tailings dams during earthquakes are nearly all attributed to the development of high pore water pressure and/or liquefaction within the body of the tailings deposit. For example, all eleven (11) tailings dam failures during the Chilean earthquake of 1965 were preceded by the liquefaction of the retained material.

Seismically-induced failures in Chile at the Barahona (1928) and El Cobre (1965) tailings dams resulted in over 250 deaths. In Japan, two of the Mochikoshi tailings dams failed during a 1978 earthquake, causing severe environmental pollution in which the flow of cyanide-laden tailings polluted a river for about 30 kilometers and destroyed the marine life in a bay.

In some cases, the consequences of failure can be disastrous both from physical and environmental losses. There are many other non-documented cases, where a failure results in only a temporary loss of storage to a mining company. In Table 2.4 is summarized some of the available information on the characteristics of seismic failures of tailings dams.

In the next two sections, are presented two of the more prominent and well-documented catastrophic tailings dam failure incidents namely, the El Cobre and Mochikoshi tailings dams.

2.3.1 El Cobre Tailings Dam

During the La Liqua earthquake of 1965 in Chile, two of three dams at the El Cobre site were almost completely destroyed. As a result, more than 2,000,000 tons of tailings flowed 12 kilometers into the valley in a few minutes, destroying part of the town of El Cobre and killing over 200 people (Dobry and Alvarez, 1967).

Copper tailings had been deposited at the El Cobre site since 1930. The Old Dam and the New Dam were 35 m and 15 m high, respectively, at the time of the failure. During the construction of these two dams, the coarser fractions of tailings settled near the edge to

Table 2.4 List of Seismic Failures of Tailings Dams

Name and Location of Dam	Year	Consequences due to F ..ure	Type of Dam	Height of Dam (m)	Volume Flow ·1 (tons)	Distance Inundated (km)	Source
Barahona, Chile	1928	54 killed	Upstream	61	4,000,000	n/a	Dobry and Alvarez (1967)
Old El Cobre, Chile	1965	210 killed	"	35	2,000,000	12.0	" "
New El Cobre, Chile	1965	-	"	15	500,000	12.0	" "
Hierro Viejo, Chile	19[illegible]	pollution	"	5	1,200	1.0	" "
Los Maquis, Chile	1965	pollution	"	15	30,000	5.0	" "
La Patagua, Chile	1965	pollution	"	15	50,000	5.0	" "
Cerro Negro, Chile	1965	pollution	"	20	120,000	5.0	" "
Bellavista, Chile	1965	pollution	"	20	100,000	2.5	" "
Ramayana, Chile	1965	pollution	"	5	200	n/a	" "
Mochikoshi, Japan							Marcuson et al. (1979)
Dam No. 1	1978	pollution	"	32	140,000	30.0	" "
Dam No. 2	1978	pollution	"	24	5,250	0.25	" "

form the shell (i.e., the starter dam and secondary dams) and the slimes flowed inward towards the pond. When the slimes settled out, free water was ponded on top. The existing front slope of the Old Dam receded 65 m, producing an almost vertical scarp. After the earthquake, all the unconsolidated tailings flowed out leaving a terraced deposit of the somewhat more consolidated tailings behind, as shown in Fig. 2.6.

According to the study carried out by Dobry and Alvarez (1967), it was confirmed that the mechanism of failure, in both the Old and New Dams, was the liquefaction of the retained tailings which then exerted greater horizontal pressure on the shell of the tailings deposit. The increased pressure on the shell was probably sufficient to induce failure in this upstream construction type of tailings dam, especially since liquefaction of the tailings may also have removed support from the shell. It was further believed that the shell itself may also have liquefied in its zone of saturation.

2.3.2 Mochikoshi Tailings Dams

The Mochikoshi tailings dams failed as a result of the January 14, 1978 major

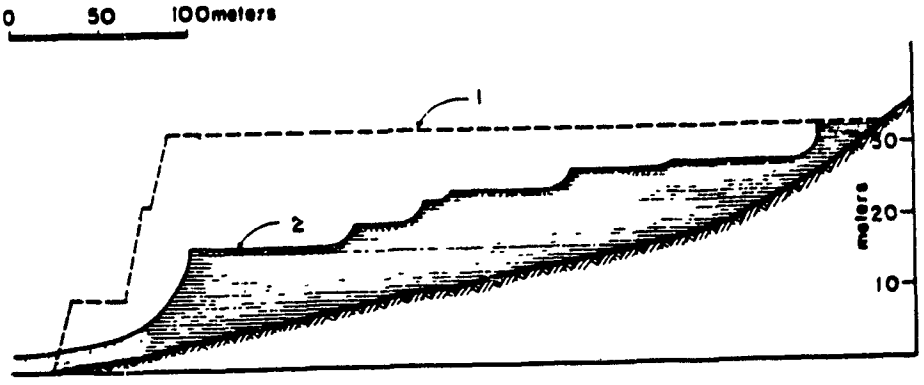

(1) Profile before failure. (2) Profile after failure.

Figure 2.6 El Cobre Old Dam. Before and After The Failure (Finn, 1981).

earthquake, of magnitude 7.0, in the nearby area of Izu-Oshima, Japan (Marcuson et al., 1979). Of the three dams constructed by the upstream method and retaining tailings from the gold mining and refining operations, two collapsed.

Tailings were deposited in a bowl-shaped structure on top of a mountain in the center of the Izu Peninsula. The bowl was sealed off by three dams, and the two failed dams, namely the Nos. 1 and 2 dams, were 32 m and 24 m high, respectively, before failure. A plan view of the site is shown in Fig. 2.7, indicating the area involved in flow slides. The cross-sections of the dams which failed, i.e., Dam Nos. 1 and 2, are shown before and after their failure in Fig. 2.8.

During the main earthquake shock which occurred at 12:24 p.m. on January 14, 1978, the No. 1 dam failed over a width of 73 m and a depth of 14 m. As a result of this dam failure, a total volume of 80,000 m^3 was released, of which 60,000 m^3 was the sodium cyanide-contaminated tailings and 20,000 m^3 the dam-forming volcanic ashes. A

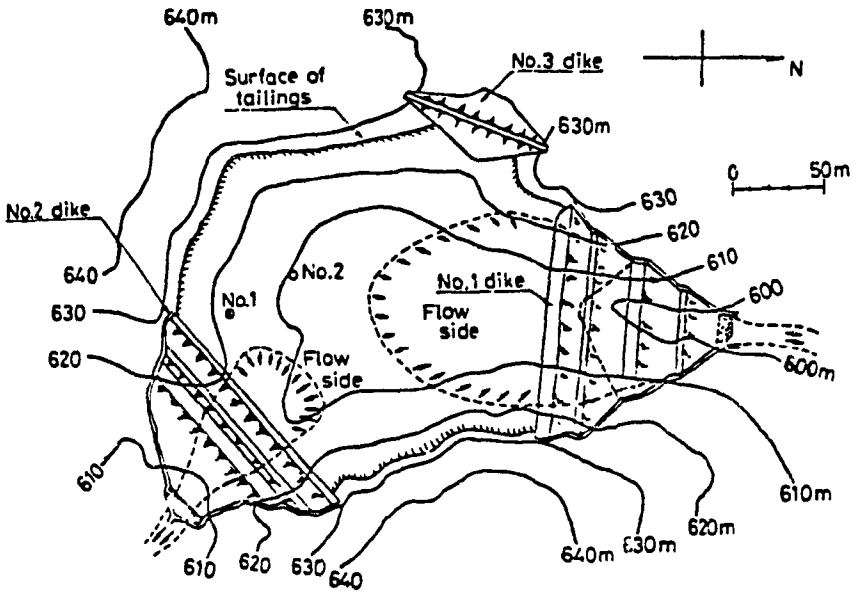

Figure 2.7 Plan View of Mochikoshi Tailings Dams Site (Finn, 1981).

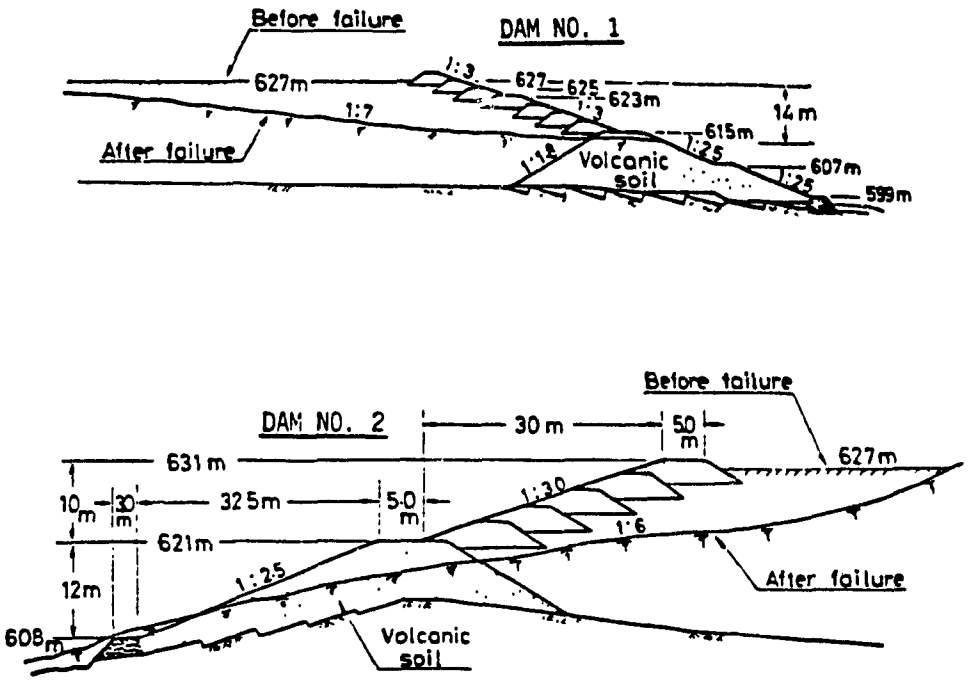

Figure 2.8 Cross-Sections of Dam Nos. 1 and 2. Before and After The Failure (Finn, 1981).

portion of the liquefied mass flowed down the mountain, polluting the Mochikoshi River and destroying the marine life in a bay located about 30 km from the site.

The No. 2 dam, however, did not fail until about 12:50 p.m. on January 15, 1978, approximately 24 hours after the occurrence of the initial main earthquake shock. Although a large aftershock of magnitude 5.7 occurred at 7:32 a.m. on January 15, 1978, it is believed that it but only contributed to the delayed failure of the No. 2 dam, which was begun by the initial main shock. This dam failed over a width of 55 m and a depth of 12 m and about 2,000 - 3,000 m^3 of tailings were released into the river.

It was found by Marcuson et al. (1979), that the tailings in the No. 2 dam liquefied early during the initial main earthquake. Liquefaction of the retained material created high pore water pressures within the body of the dam and/or removed the support from the 3 m

high secondary dams making up the shell. These two factors were considered to be responsible for the belated failure of this dam.

Finally, it is clear that the experiences of these earthquakes confirms the great seismic instability of upstream construction type of tailings dams.

CHAPTER 3

FORMULATION OF THE PROBLEM

3.1 Introduction

In this chapter is presented the formulation of the problem in order to obtain the phreatic surface solution and the corresponding pore water pressure distribution within a tailings dam. A description of the computer program written for this study together with its verification for correctness are also contained.

3.2 Governing Equations and Assumptions

In a porous medium such as a tailings dam, the length of the dam is many times larger than its cross-sectional dimensions. It is therefore reasonable to disregard all flow perpendicular to the plane of the cross-section, i.e., the z-plane. This means that the head, h, may be assumed to be independent of z (i.e., $h = h(x,y)$).

The fundamental two-dimensional problem of seepage through a saturated, isotropic, and inhomogeneous porous medium can be formulated by the following set of equations (Desai, 1972):

$$\partial/\partial x\,(k\,\partial h/\partial x) + \partial/\partial y\,(k\,\partial h/\partial y) + Q = \eta\,\partial h/\partial t \qquad (\text{in } R) \qquad (3.1)$$

$$h = f \qquad (\text{on } S_1) \qquad (3.2)$$

$$q_n = -k\,\partial h/\partial n \qquad (\text{on } S_2) \qquad (3.3)$$

where $S_1 + S_2$ is the entire boundary of the region R, and $\partial/\partial n$ is the derivative perpendicular to the boundary, the outward direction being considered as positive. In equation 3.1:

k = coefficient of permeability in both the x and y directions

t = time

$h = p/\gamma_w + y$ = total hydrostatic head or potential

p = pressure head

γ_w = unit weight of water

y = elevation head

η = porosity of the medium

Q = externally applied fluid flux

q_n = prescribed fluid flux input

Equation 3.2 is the boundary condition along the part of the boundary (S_1) where the head is prescribed. Equation 3.3 is the boundary condition along the part of the boundary (S_2) where a given flux, q_n, is applied into the medium. It should be noted that in a tailings deposit, the permeability coefficient, k, in the x and y directions may not be equal due to the fact that the construction procedures cause stratification of the deposited layers to occur. However, for the purpose of this study, it will be assumed that the permeability coefficients in the x and y directions are the same.

For steady-state flow, the right-hand side in equation 3.1 vanishes and, for no externally applied fluid flux we are left with:

$$\partial/\partial x \, (\, k \, \partial h/\partial x \,) + \partial/\partial y \, (\, k \, \partial h/\partial y \,) = 0 \qquad (3.4)$$

Further, because of the existence of a free surface in steady unconfined flows we must consider the following boundary conditions (refer to Fig. 3.1):

$$h = D \text{ on } 1 - 2 \qquad (3.4a)$$

$$h = H \text{ on } 2 - 3, p = 0 \qquad (3.4b)$$

$$h = y \text{ on } 3 - 4, p = 0 \qquad (3.4c)$$

$$h = d \text{ on } 4 - 5, p = 0 \qquad (3.4d)$$

$$\& \quad \partial h/\partial y = 0 \text{ on } 1 - 5 \qquad (3.4e)$$

Equations (3.4a) and (3.4d) are equivalent to equation (3.2), i.e., the boundary conditions along the parts of the boundary where the head is prescribed. We also notice that

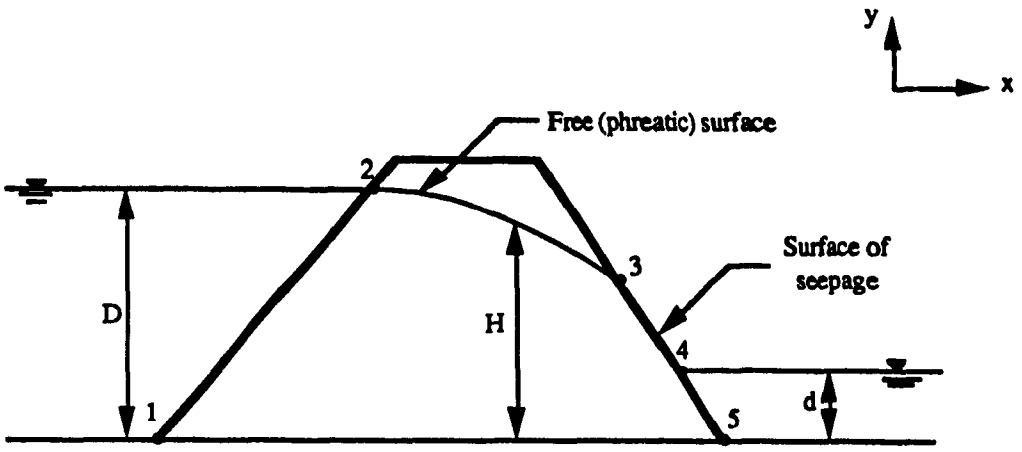

Figure 3.1 Example of Steady Unconfined Flow with a Free Surface.

the conditions in equations (3.4b) and (3.4c) are due to the free (phreatic) surface and that the region 3-4 constitutes the surface of seepage. Furthermore, equation (3.4e) is a special case of equation (3.3) stating that the flow across the surface 1-5 is equal to zero.

3.3 Finite Element Formulation

The basic techniques of the finite element method can be established by using a variational formulation of the problem. In our problem, we have steady-state flow without any externally applied or prescribed fluid flux, i.e., $Q = 0$ and $q_n = 0$, respectively. Thus, the variational principle equivalent to equation (3.4) is as follows.

As shown by Verruijt (1982), a functional U may be defined by :

$$U = 1/2 \int_R \int [\, k\, (\, \partial h/\partial x\,)^2 + k\, (\, \partial h/\partial y\,)^2 \,]\, dxdy \qquad (3.5)$$

with the constraint

$$h = f \qquad (\text{on } S_1) \qquad (3.6)$$

such that the functional U possesses an absolute minimum for the function h that satisfies

the equations 3.1 to 3.3.

In the finite element method the region R is subdivided into a great number of elements. Then,

$$U = \sum_{j=1,m} U_j \tag{3.7}$$

where U_j represents the integral over a single element, and where m is the number of elements. A simple and yet flexible form of subdividing the region R is by using triangular elements. The values of the head, h, in the nodes are taken as the free parameters in the problem, and in the interior of each element a linear interpolation between the values in the three corner points is used. This means that in a typical element R_j

$$h = p_1 x + p_2 y + p_3 \tag{3.8}$$

It seems reasonable to require that the approximation $h = h(x,y)$ of the fluid head is continuous. In combination with the linear interpolation rule in equation (3.8), this means that the function $h(x,y)$ is approximated by a diamond-shaped surface with many facets (Verruijt, 1982).

If the node numbers of the typical element R_j are denoted by 1, 2 and 3, at least temporarily, the condition that the head, h, should be continuous leads to the equations:

$$\begin{aligned} h_1 &= p_1 x_1 + p_2 y_1 + p_3 \\ h_2 &= p_1 x_2 + p_2 y_2 + p_3 \\ h_3 &= p_1 x_3 + p_2 y_3 + p_3 \end{aligned} \tag{3.9}$$

This means that the three parameters p_1,p_2 and p_3 can be expressed into h_1,h_2 and h_3 by the relations:

$$\begin{aligned} p_1 &= (b_1 h_1 + b_2 h_2 + b_3 h_3)/\Delta \\ p_2 &= (c_1 h_1 + c_2 h_2 + c_3 h_3)/\Delta \\ p_3 &= (d_1 h_1 + d_2 h_2 + d_3 h_3)/\Delta \end{aligned} \tag{3.10}$$

where

$$b_1 = y_2 - y_3\,,\quad b_2 = y_3 - y_1\,,\quad b_3 = y_1 - y_2 \tag{3.11}$$

$$c_1 = x_3 - x_2\,,\quad c_2 = x_1 - x_3\,,\quad c_3 = x_2 - x_1 \tag{3.12}$$

$$d_1 = x_2y_3 - x_3y_2\,,\quad d_2 = x_3y_1 - x_1y_3\,,\quad d_3 = x_1y_2 - x_2y_1 \tag{3.13}$$

and where Δ is the determinant of the system of linear equations (3.9), that is

$$\Delta = x_1b_1 + x_2b_2 + x_3b_3 \tag{3.14}$$

It is to be noted that the quantities b_i , c_i , d_i and Δ can easily be calculated if the coordinates of the three nodes of the element R_j are known.

It follows from equation 3.8 that in element R_j the values of $\partial h/\partial x$ and $\partial h/\partial y$, which are needed in the integral, are constants. Hence

$$U_j = 1/2 \int_{Rj}\int [\, k\,(\,p_1^2 + p_2^2\,)\,]\, dxdy$$

In this integral p_1 and p_2 are constants. If it is assumed that in each element the permeability, k, is constant, say $k = k_j$ in R_j, then all that remains is to evaluate the area of the triangle, which can be shown to be equal to $1/2\,|\Delta|$. Thus the value of U is:

$$U = 1/4\;\; k_j\,|\Delta|\;\,(p_1^2 + p_2^2) \tag{3.15}$$

With the first two parts of equation (3.10) this can be elaborated into:

$$U_j = 1/2\;\; \sum_{l=1,3} \sum_{m=1,3} P^j_{lm}\;\, h_l\, h_m \tag{3.16}$$

where P^j is a 3x3 matrix with coefficients:

$$P^j_{lm} = 1/2\;\; k\,|\Delta|\;(\,b_lb_m + c_lc_m\,) \tag{3.17}$$

The nine coefficients of this matrix can easily be calculated from the geometrical data describing the element (the coordinates of the nodes) and from the permeability, k_j, which is also supposed to be given.

From each element R_j there will be a contribution to the functional U in the form of

equation (3.16), quadratic in the variables h_l. After summation over all elements a quadratic form for U is obtained:

$$U = 1/2 \ \Sigma_{l=1,n} \Sigma_{m=1,n} P_{lm} \ h_l h_m \tag{3.18}$$

where n is the total number of nodes. The calculation of the matrix coefficients P_{lm} are performed by computer whereby a program is written such that it generates its coeffients on the basis of elementary matrices of the form of equation (3.17).

The minimum value of U occurs for those values of h_l for which

$$\partial U/\partial h_i = 0 \ , \ i = 1, 2, 3, ..., n \tag{3.19}$$

With equation 3.17 this leads to the following system of equations:

$$\Sigma_{l=1,n} P_{il} \ h_l = 0 \ , \ i = 1, 2, 3, ..., n \tag{3.20}$$

where use has been made of the symmetry of the matrix ($P_{lm} = P_{ml}$). The unknown variable h_m is determined from equation (3.20) by a standard subroutine of solving a system of linear equations.

It should be noted that not all values h_m are unknown. In some nodes the value of h is prescribed through the boundary condition, which is in fact the constraint in equation (3.6), which is imposed on these variables.

3.4 Computer Program PWP

A computer program called PWP was written, incorporating the governing equations and finite element formulation described above, to determine the phreatic (free) surfaces and the corresponding pore water pressure distribution within a tailings dam on an impermeable foundation for pre-earthquake conditions and post-liquefaction conditions. The program was written in FORTRAN, based on flow charts prepared by Weaver and Johnston (1984) for structural analysis which were modified for seepage analysis and, used on an IBM-compatible personal computer.

The computer program named PWP includes six (6) subroutines. The subroutines, in order of calling by program PWP, are SDATA, STIFF, LDATA,SKYFAC, SKYSOL and RESUL. A copy of program PWP and its subroutines is presented in Appendix A and brief descriptions of the main program and the subroutines are included.

In order to obtain the correct pore water pressure distribution within a given porous medium requires that the location of the phreatic surface, which is initially unknown, be determined. The fact that the location of the phreatic surface is initially unknown is overcome by using a manual iterative process of program PWP.

The location of the phreatic surface is estimated, for example in the shape of a straight line, and it is considered as a 'stream line', ignoring the condition that the groundwater head should equal the elevation (because $p = 0$). The distribution of the pore water pressure within the discretized region(s) is then calculated by means of the finite element method using program PWP. At the end of each run of the computer program, the calculated head, h, along the estimated phreatic surface is compared with the elevation y. If these values are not equal, to within say 1%, a new estimation for the phreatic surface is made by changing the position (elevation) of the existing nodes on the estimated phreatic surface and/or by removing or placing additional elements should the change in positions of the nodes be too excessive and cause extreme distortions within the mesh. This mode of manual iteration is repeated until the final estimation of the phreatic surface is acceptable.

The pore water pressure distribution within the discretized region is calculated during every run of program PWP. However, only upon obtaining the final phreatic surface solution do we obtain the correct pore water pressure distribution within the discretized region for the imposed boundary conditions.

3.5 Verification of Program PWP

To verify that program PWP solves for the correct (final) phreatic surface for any discretized region within a porous medium, program PWP was initially used to solve for

the location of the phreatic surface in a simplified water storage dam problem on an impermeable foundation in which, the phreatic surface was previously solved both analytically and by using another computer program based on the finite element method. The solution for the final phreatic surface, obtained using program PWP, was then compared with the known analytical solution (Muskat, 1937) and the known solution obtained using another computer program (Verruijt, 1982).

The external boundary conditions imposed on the simplified water storage dam are the following (refer to Figs. 3.2 & 3.4):

$h = D$	on face 1 - 2
$h = H$	on phreatic surface 2 - 3
$h = y$	on surface of seepage 3 - 4
$h = d$	on face 4 - 5

For this simplified water storage dam, the initial guess at the phreatic surface is estimated to be a straight line from the upstream face of the dam to the downstream face of the dam, as shown in Fig. 3.2. Also shown, is the finite element mesh for this initial estimate of the phreatic surface.

For this first iteration using program PWP, the values from the output indicate that the initial guess at the phreatic surface is too low and therefore, the next estimation for the phreatic surface must be adjusted relatively higher. This process is repeated until the preceding estimate to the phreatic surface (i.e., input data) and the output of the calculated pore water pressure are in close agreement, that is, less than 1%. The final phreatic surface obtained using program PWP together with the finite element mesh are shown on Fig. 3.3. It should be noted that additional finite elements were added to the original mesh since the change in elevation from the initial guess to the final solution was very large.

In Fig. 3.4, shown superimposed, are the final phreatic surface solutions obtained by Muskat (1937), Verruijt (1982) and program PWP. As can be seen, the solution obtained using the manual iterative method of program PWP is in close agreement to both

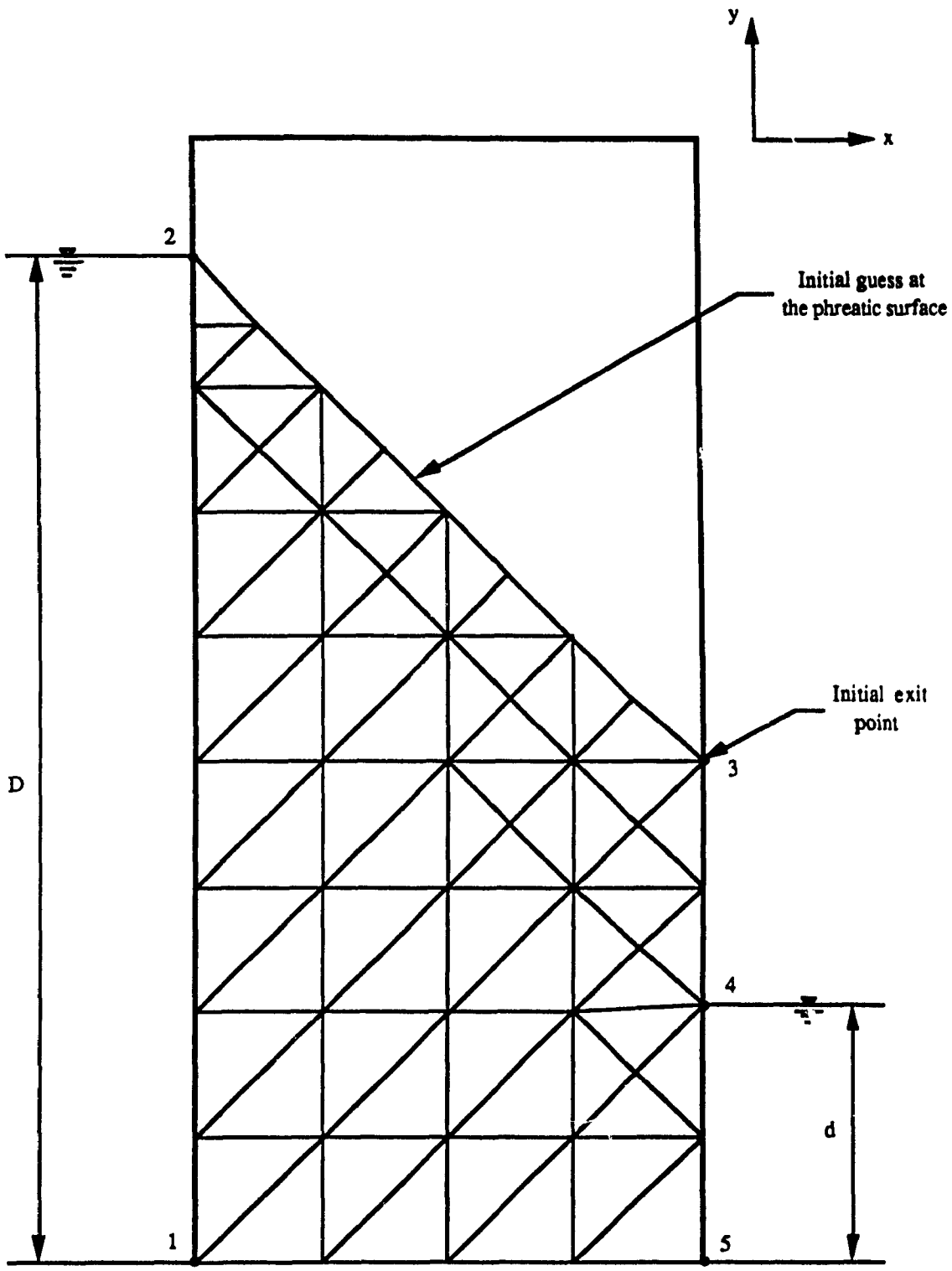

Figure 3.2 Verification Dam: Initial Guess Line of the Phreatic Surface.

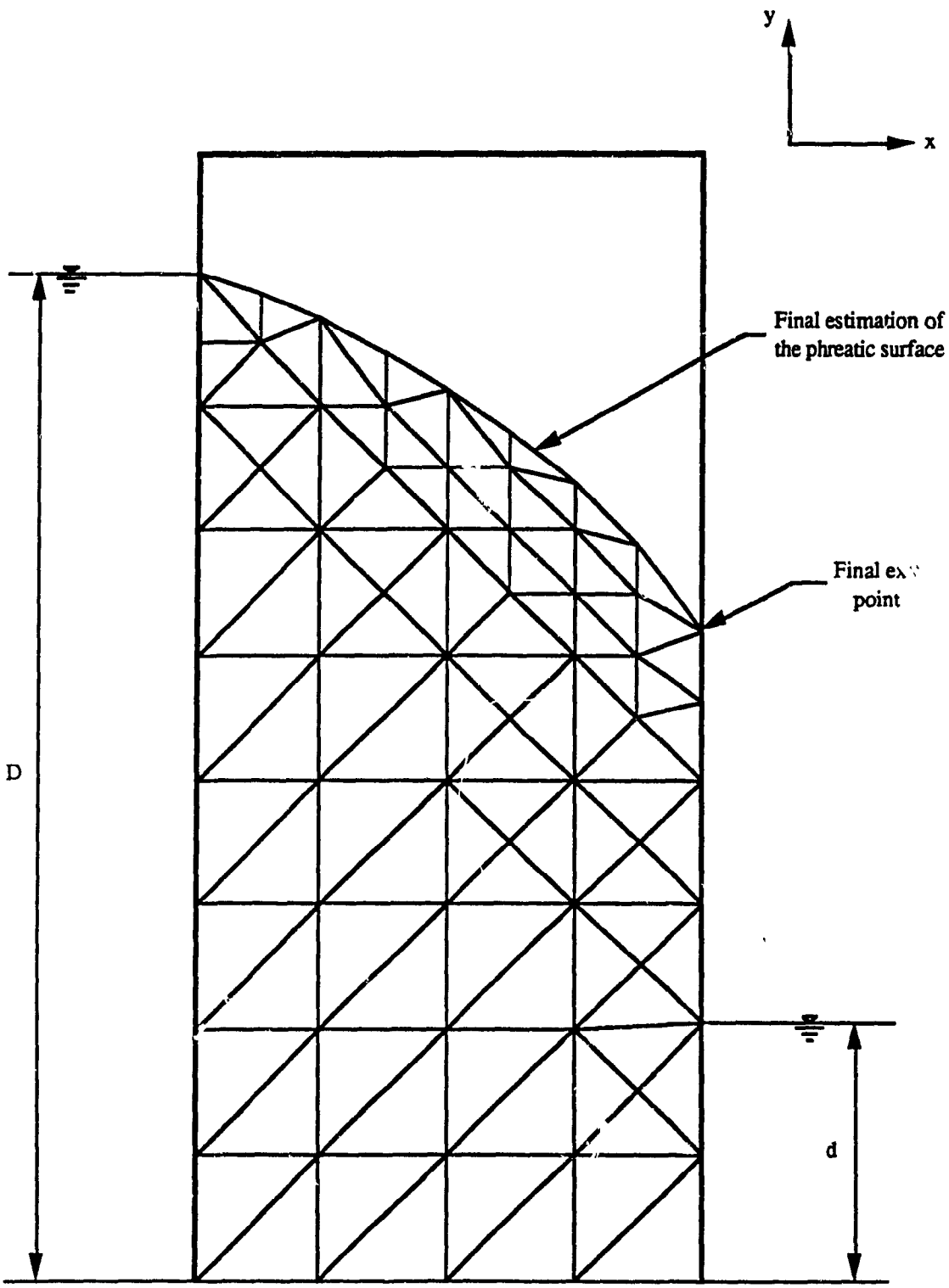

Figure 3.3 Verification Dam: Final Estimation of the Phreatic Surface.

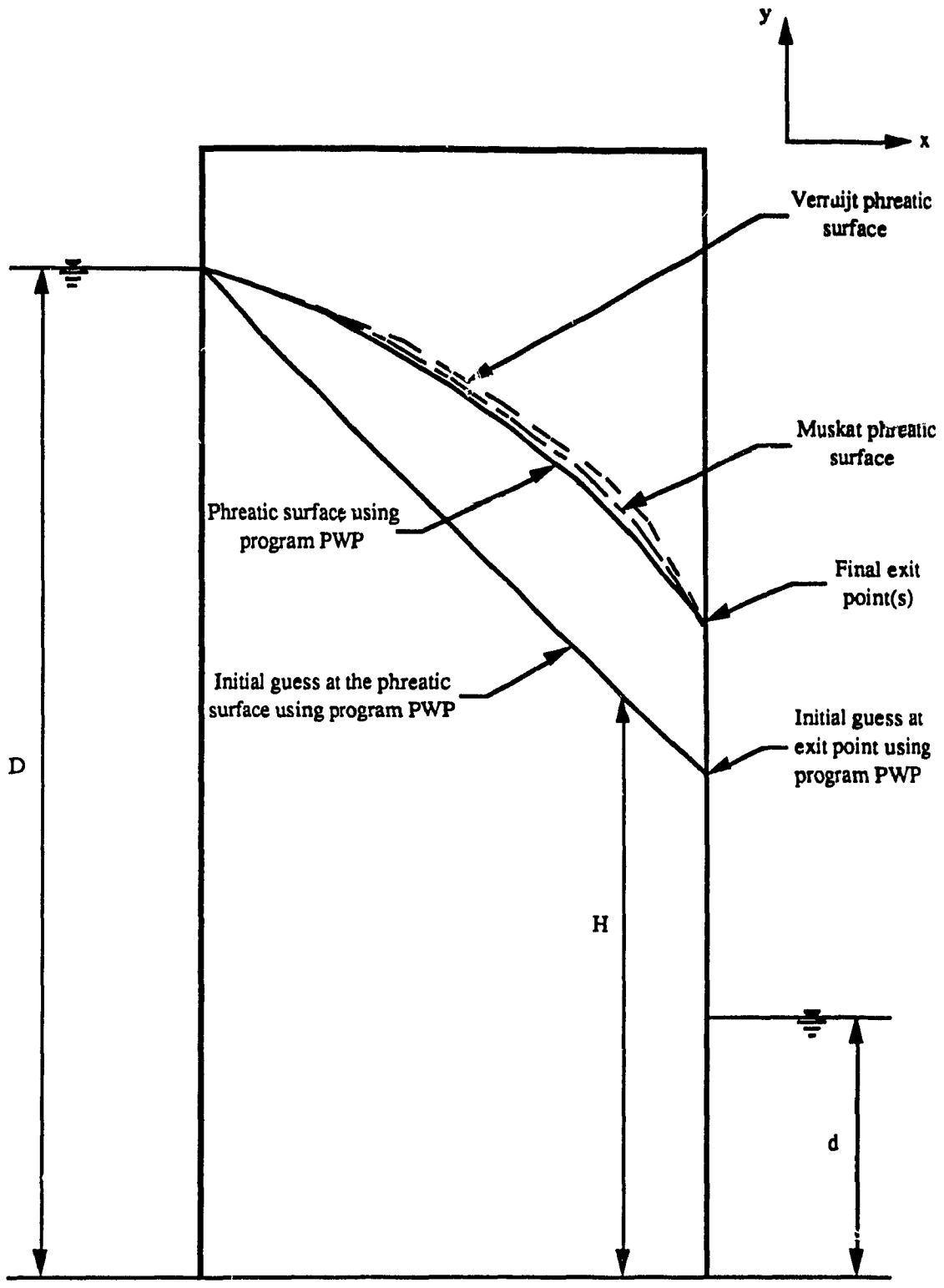

Figure 3.4 Verification Dam: Comparison of Different Solutions of the Phreatic Surface.

of the other two previously determined phreatic surface solutions. Hence, it may be concluded that program PWP provides a solution for the phreatic surface and subsequently for the pore water pressure distribution which are quite satisfactory.

CHAPTER 4

PHREATIC SURFACE SOLUTIONS AND PORE WATER PRESSURE DISTRIBUTIONS

4.1 Introduction

As mentioned in Section 2.1.1, the upstream, downstream and centerline methods are the type of construction methods commonly used for tailings dams. Of these three, the upstream type of tailings dam is the one most likely to fail when subjected to a severe earthquake. This is due to the fact that the upstream method requires secondary dams to be built on top of the previously deposited, fine, saturated, and unconsolidated tailings.

During periods of strong ground motion, the finer retained tailings will tend to liquefy thereby decreasing and/or removing the support for the secondary dams situated above. More importantly, the liquefaction of the tailings will result in an initial increase of the pore water pressure within the retained deposit and, after a while, within the relatively thin shell of the tailings dam, comprising the starter dam and secondary dams. This sequence of events may lead to instability of the tailings dam structure and cause a partial and/or complete failure of the system.

In this chapter, the phreatic surfaces within an upstream construction type of tailings dam will be determined for pre-earthquake conditions and post-liquefaction conditions using program PWP. Also, the pore water pressure distribution within the body of the tailings dam for both cases will be presented.

4.2 Pre-Earthquake Case

The pre-earthquake case represents the state and condition of the entire tailings deposit prior to the liquefaction of the retained material, as may occur due to a severe earthquake. The upstream type of tailings dam that will be analyzed in this study shall

consist of a starter dam and two typical secondary dams, as shown in the schematic representation in Fig. 4.1.

Although many different variations in the shapes and sizes of the starter dam, secondary dams and retained tailings deposit exist, for the purpose of this study the simplified and typical upstream type of tailings dam shown in Fig. 4.1 will be analyzed. The information required for the selection of this typical upstream type of tailings dam was obtained from a number of references listed at the end of this thesis.

4.2.1 Boundary Conditions and Assumptions

In the schematic representation of the upstream type of tailings dam, the level of the water in the tailings pond is assumed to coincide with the top surface of the uppermost secondary dam. In order to simplify the numerical representation of the imposed head boundary conditions and the analysis of the calculated heads, it is assumed that the height of the tailings deposit is scaled equal to 10 units. Hence, the external boundary conditions imposed on the tailings deposit are the following (refer to Fig. 4.1):

$h = 10.0$	on face 1 - 2
$h = 10.0$	on face 2 - 3
$\& \ \partial h/\partial y = 0$	on face 3 - 4 and, bottom boundary of the tailings dam

As shown in Table 2.1, the average coefficient of permeability of tailings varies over several orders of magnitude. Clean, coarse sands with less than 15% fines, usually the type of tailings used to construct the body of the tailings dam, have permeability coefficients in the range of 10^{-2} to 10^{-4} cm/sec. The average coefficient of permeability of the retained tailings (slimes) depends on the distance away from the body of the tailings dam and, may vary between 10^{-4} to 10^{-6} cm/sec. Hence, for this study we will assume that the average permeability coefficient of the sands comprising the body of the tailings dam is approximately 100 times greater than the average permeablity coefficient of the retained

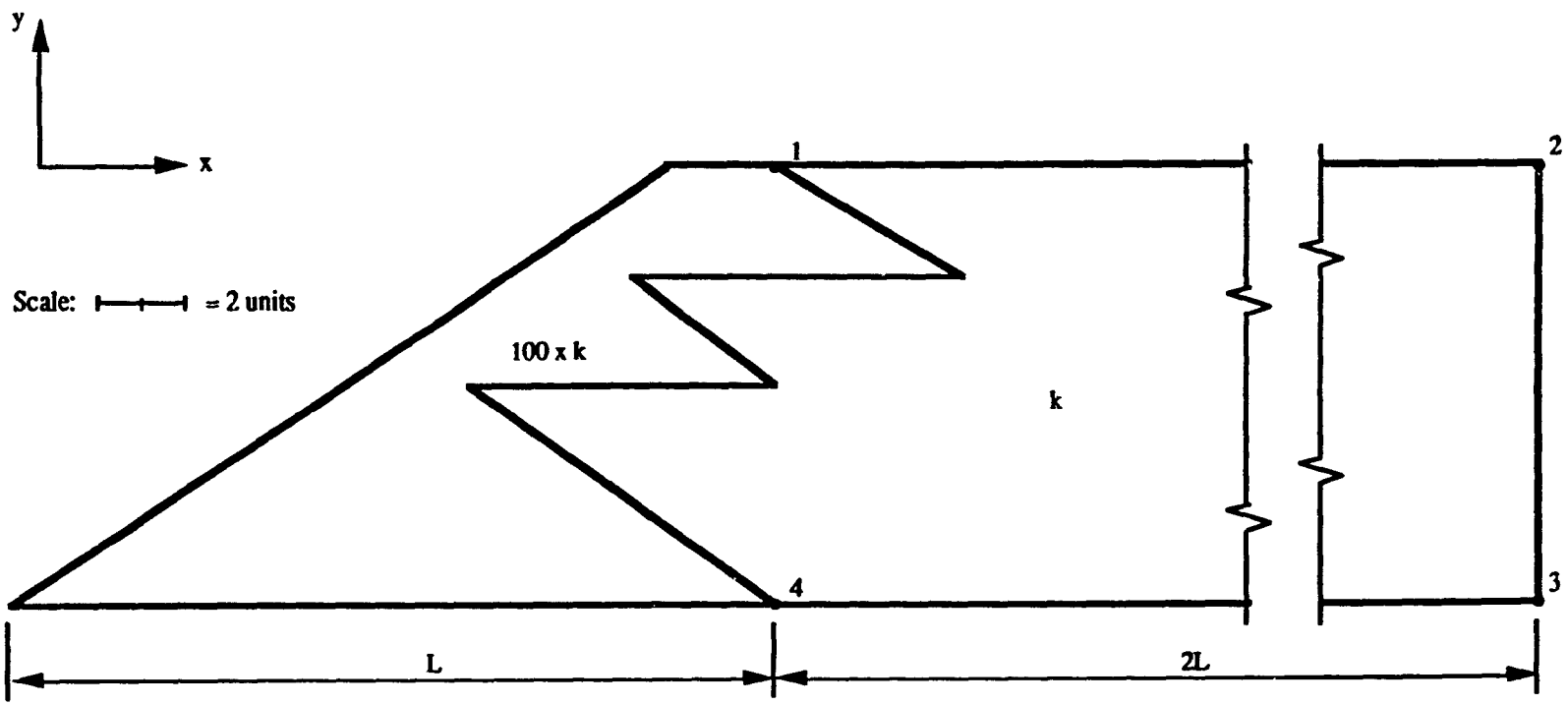

Figure 4.1 Boundary Conditions for Pre-Earthquake Case.

tailings (slimes), i.e., $k_{sands} = 100 \times k_{slimes}$.

In general, the length in cross-section of the entire tailings deposit is much larger than its height. In order to quantify the length in cross-section, the base of the starter dam has been assigned a length of distance L and the retained deposit has been assigned a length of distance $2L$. The length of $2L$ was assumed for the retained deposit because, as shall be mentioned later, it provides a satisfactory solution.

4.2.2 Phreatic Surface Solution

As discussed in Section 3.4, an initial guess at the phreatic surface, in the shape of a straight line, is taken from the top-upstream corner of the uppermost secondary dam to an exit point located near the toe of the starter dam (refer to Fig. 4.2). According to the discussion in the preceding section, the average coefficients of permeability of the retained slimes and the sands comprising the tailings dam are k and $100 \times k$, respectively.

The finite element method mesh discretization of the entire tailings deposit is performed ensuring that a division between the regions of different permeabilities (i.e., the tailings dam and the retained deposit) is maintained. Further, in order to decrease the complexity and fineness of the mesh and also, to reduce the amount of computer time required to run program PWP, a minimum number of elements have been employed while creating the mesh. However, for flexibility purposes, a sufficient number of nodes were placed on the initial guess line of the phreatic surface and on each subsequent estimation of the phreatic surface during the manual iteration process. That is, so that the relative increases and/or decreases in the position of the nodes on the estimated phreatic surface between any two iterations may be satisfactorily accommodated in order to attain an acceptable solution for the shape of the phreatic surface.

After each iterative step, the elevations (input data) of the nodes on the estimated phreatic surface were compared with the calculated heads (output results) of these nodes obtained using program PWP. Accordingly, in some cases, the number of finite elements

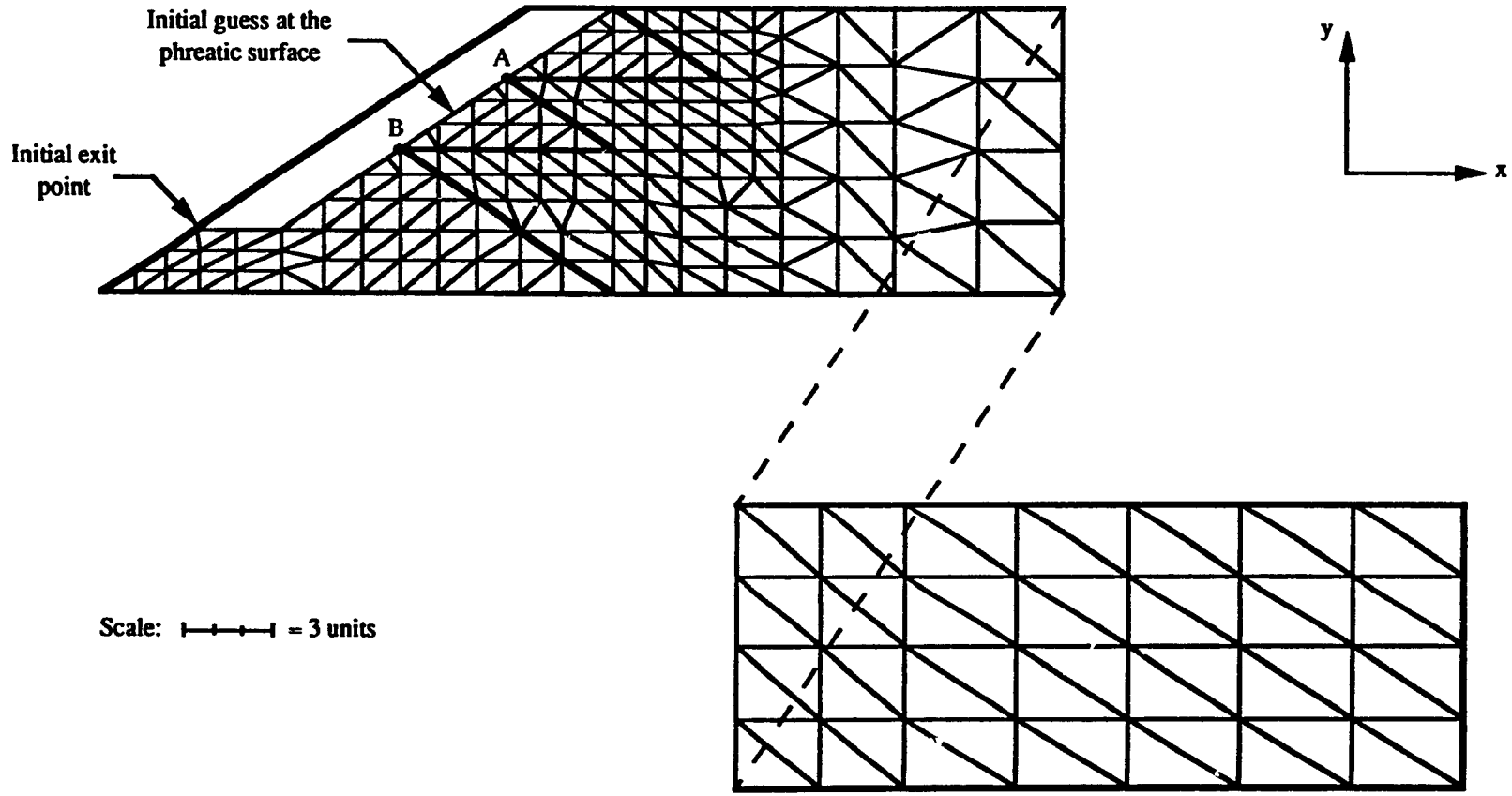

Figure 4.2 Pre-Earthquake Case: Initial Guess at the Phreatic Surface.

in the body of the tailings dam was varied depending on the amount of relative change in the position of nodes necessary on the estimated phreatic surface. It is for this reason that a manual iterative method for the mesh generation and modification is utilized.

After several manual iterations, including varying the number of elements and conducting numerous modifications on the location of the nodes, the final phreatic surface solution for the pre-earthquake case is obtained, as shown in Fig. 4.3. Modifications were carried out mainly on and/or near the estimated phreatic surface, as well as near two critical points. The two critical points, indicated by points A and B on Figs. 4.2 and 4.3, are located on the boundary between the tailings dam and the retained deposit where the estimated phreatic surface intersects two elements having different coefficients of permeability.

During many seperate iterations, in order to determine the correct location of the phreatic surface, the phreatic surface was estimated to pass above, through, and/or below the two critical points, A and B. After several different iterations and alterations in the number and size of elements and the relative change in the level of nodes on the estimated phreatic surface, it was found that the phreatic surface passes very close to these two critical points. Hence, for our practical purposes it has been assumed that the phreatic surface passes through both of these two points.

The determination of the location of the final exit point for the phreatic surface on the downstream slope of the tailings dam required that the iteration process take into account the fact that the phreatic surface, especially near the exit point, be entirely confined within the body of the tailings dam. This dilemma was solved by progressively increasing the height of the exit point until the phreatic surface solution was placed outside the body of the tailings dam. Then, the previous estimate for the location of the exit point, for which the entire phreatic surface was located within the tailings dam, was assumed to be correct.

The final phreatic surface was considered satisfactory when the difference between the elevation and the calculated head of any point on the estimated phreatic surface was less

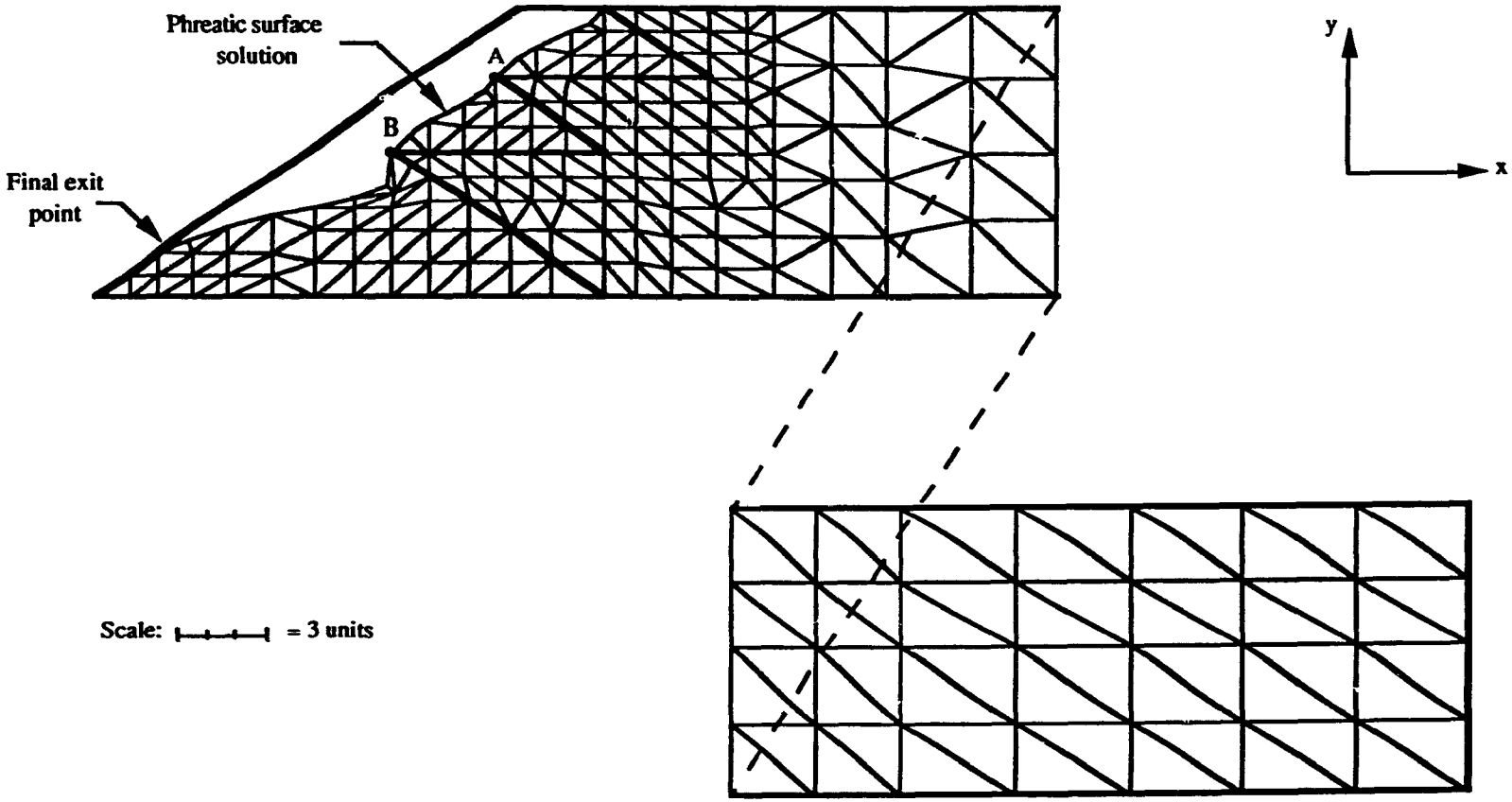

Figure 4.3 Pre-Earthquake Case: Phreatic Surface Solution.

than 1%.

Finally, to verify that the length of $2L$ for the retained deposit did not have any significant bearing on the final solution obtained for the phreatic surface, another run of program PWP was performed using a length of $3L$ for the retained deposit. The calculated heads of the nodes on the phreatic surface for this run (i.e., $3L$) were then compared to the previous results (i.e., $2L$) and the difference between the two runs was found to be less than 1%. Thus, it was shown that the length of $2L$ initially chosen for the length of the retained deposit is sufficient to simulate the conditions of the entire tailings deposit analyzed quite well.

4.2.3 Pore Water Pressure Distribution

After obtaining the phreatic surface solution for the pre-earthquake case, as described above, we also attained the pore water pressure distribution within the entire tailings deposit using the calculated head values at each node, i.e., the output obtained from program PWP. In order to better visualize the results obtained, a series of equipotential lines is plotted on the schematic representation of the tailings deposit. The pore water pressure distribution for the pre-earthquake case is shown on Fig. 4.4.

4.3 Post-Liquefaction Case

The post-liquefaction case represents the state and condition of the tailings deposit after the complete liquefaction of the retained material has occurred, as may be caused by a severe earthquake. For this case, the same upstream type of tailings deposit will be analyzed as in the pre-earthquake case.

4.3.1 Boundary Conditions and Assumptions

After the retained deposit has completely liquefied, we may safely assume that an increase in the horizontal forces acting upon the upstream face of the family of dams will

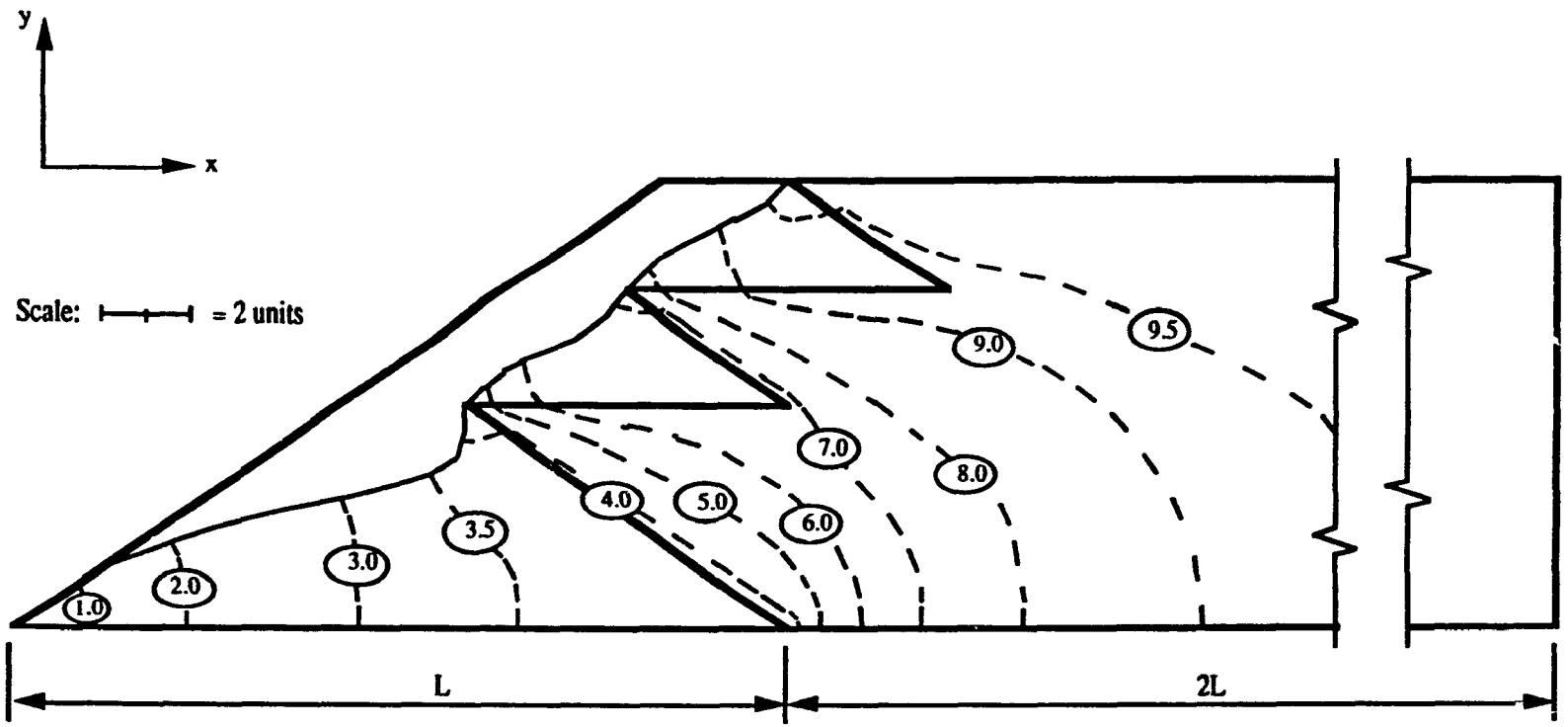

Figure 4.4 Pre-Earthquake Case: Pore Water Pressure Distribution.

occur. Furthermore, after liquefaction has occurred, and since the retained slimes are usually in a saturated state, an increase in the boundary conditions will be imposed at the bottom of the tailings dam, having a height, H, of an amount equal to

$$(\gamma'_{sat\ (slimes)} H\ ) / \gamma_w \qquad (4.1)$$

where,

$\gamma'_{sat\ (slimes)}$ = effective saturated density of the slimes

γ_w = unit density of water

Equation (4.1) represents a linear triangular increase in the inposed boundary conditions over and above the hydrostatic head due to the water in the slimes, retained by the tailings dam. The increase varies from an amount of zero at the top of the tailings dam to the above-noted increase, noted by equation 4.1, at the bottom of the tailings dam.

According to fundamental phase relationships of tailings, the total unit weight (total density), γ_t, may be defined as follows:

$$\gamma_t = ((\ G + Se\ ) / (\ 1 + e\ ))\ \gamma_w \qquad (4.2)$$

where

G = specific gravity (solids)

S = degree of saturation

e = void ratio

γ_w = unit weight of water

In our case, it is assumed that the retained material (i.e., slimes) is fully saturated, and thus S = 1.0. From Table 2.2, we can estimate that the specific gravity and void ratio for the slimes may be approximately 2.7 and 1.2, respectively. Hence, according to equation (4.2), the saturated density of the slimes, $\gamma_{sat\ (slimes)}$, is:

$$\gamma_{sat\ (slimes)} = ((\ 2.7 + (1.0)(1.2)\ ) / (\ 1 + 1.2\ ))\ (62.4)$$

$$= 110.6\ \text{pcf}$$

The increased triangular loading at the bottom of the tailings dam will thus be:

$$(\gamma'_{sat\,(slimes)} H) / \gamma_w = (\gamma_{sat\,(slimes)} - \gamma_w) H / \gamma_w$$

$$= (110.6 - 62.4) H / 62.4$$

$$= 0.76 H$$

This means that the total head, h, at each node on the upstream faces of the tailings dam will be equal to

$$h = H + 0.76 (H - y) \qquad (4.3)$$

where

H = height of the liquefied saturated deposit

y = the distance measured in the vertical direction from the bottom of the tailings dam.

Thus, for a liquefied saturated deposit of 10.0 units in height, the total head boundary conditions acting along the upstream faces of the tailings dam, as calculated using equation (4.3), are the following (refer to Fig. 4.5):

h = 10.0 to 11.9	on face 1 - 2
h = 11.9	on face 2 - 3
h = 11.9 to 13.8	on face 3 - 4
h = 13.8	on face 4 - 5
h = 13.8 to 17.6	on face 5 - 6
& $\partial h/\partial y$ = 0	at bottom boundary of tailings dam

For the boundary conditions acting on faces 1 - 2, 3 - 4 and 5 - 6, a linear interpolation between the two numerical values is assumed between the values at the extreme points for each face.

The above-noted increased boundary conditions act directly upon the faces of the tailings dam because it is assumed that the saturated retained tailings deposit has completely liquefied over its entire height. In addition, the body of the slimes has no effect on the development of pore water pressure within the body of the tailings dam. And, it is for this

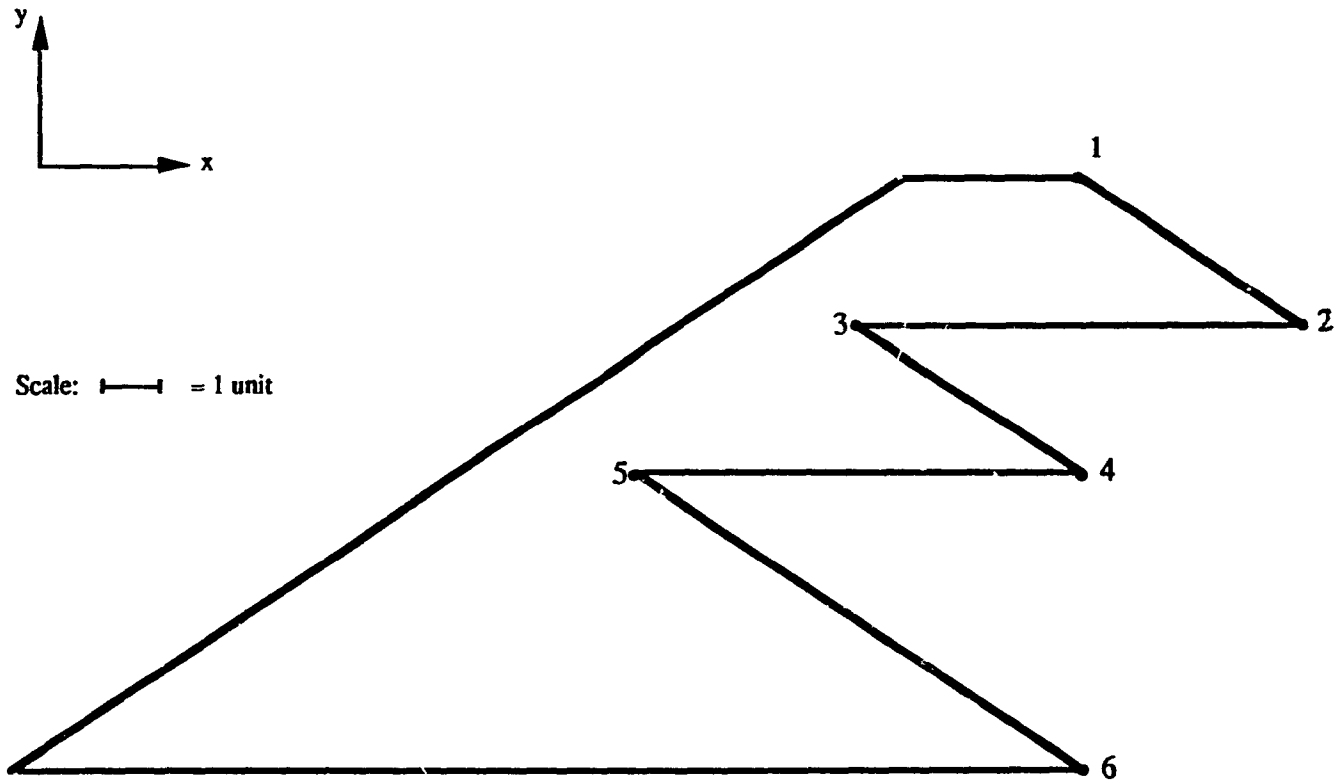

Figure 4.5 Boundary Conditions for Post-Liquefaction Case.

reason that we do not show the body of the slimes in our representation of the tailings deposit for the post-liquefaction case, as shown in Figs. 4.5 to 4.8.

4.3.2 Phreatic Surface Solution

An initial guess at the phreatic surface in the shape of a straight line, similar to the initial guess line for the pre-earthquake case, is taken for the post-liquefaction case. Next, the discretization of the dam is performed, as shown in Fig. 4.6. Similar to the pre-earthquake case, a minimum number of finite elements are utilized while still ensuring that a sufficient number of nodes are placed on the estimated phreatic surface for flexibility in modifying the elevation of the nodes located on the phreatic surface.

The output results of the first iteration for this case indicated that the entire level of the phreatic surface together with the initial exit point need to be raised in elevation. After a number of manual iterations in modifying the position of the exit point, the relative heights of the nodes on the phreatic surface, and increasing the number of elements within the body of the tailings dam, the final solution for the phreatic surface is obtained. As shown in Fig. 4.7, the location of the phreatic surface solution for the post-liquefaction case coincides exactly with the downstream slope of the tailings dam, indicating a complete saturation of the tailings dam.

4.3.3 Pore Water Pressure Distribution

The distribution of the pore water pressure for the post-liquefaction case is plotted using the results obtained from program PWP for the phreatic surface solution, as previously performed for the pre-earthquake case. A series of equipotential lines is created within the body of the tailings dam and, the pore water pressure distribution for the post-liquefaction case is shown on Fig. 4.8.

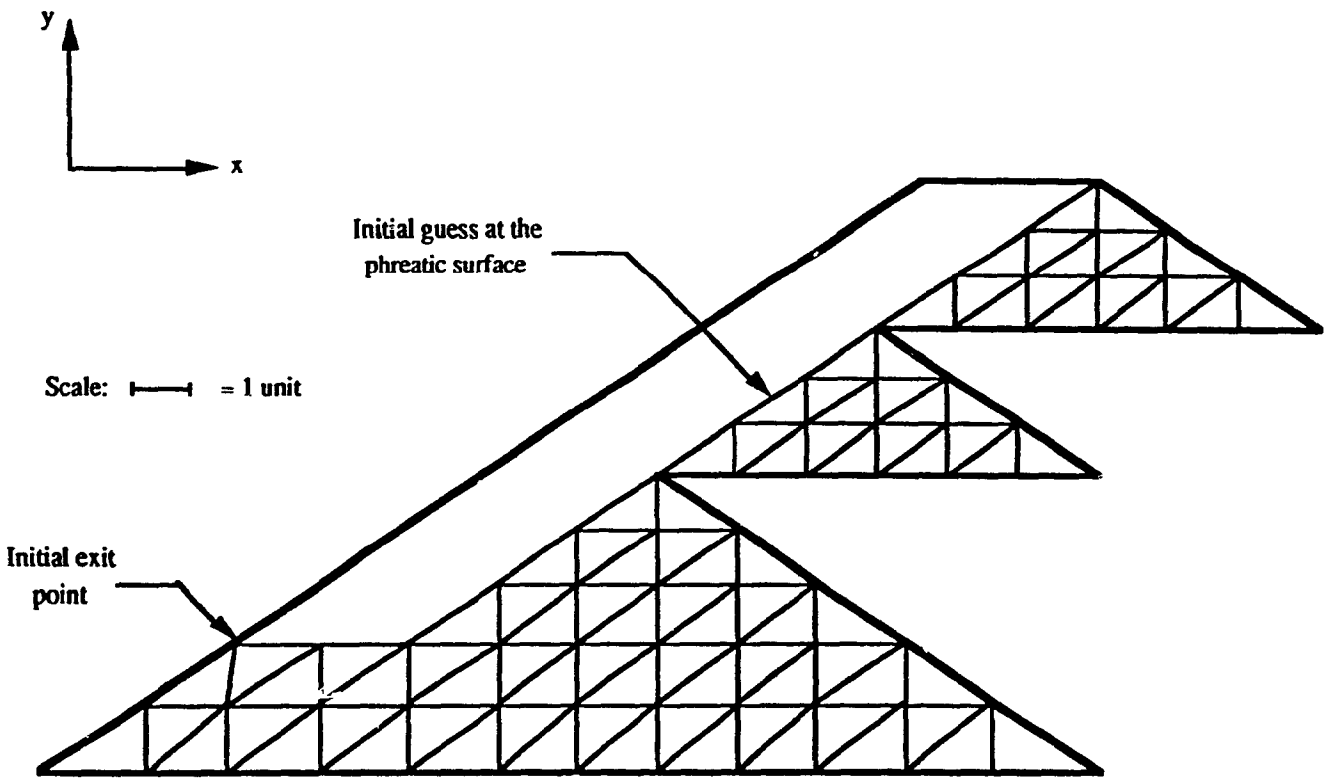

Figure 4.6 Post-Liquefaction Case: Initial Guess at the Phreatic Surface.

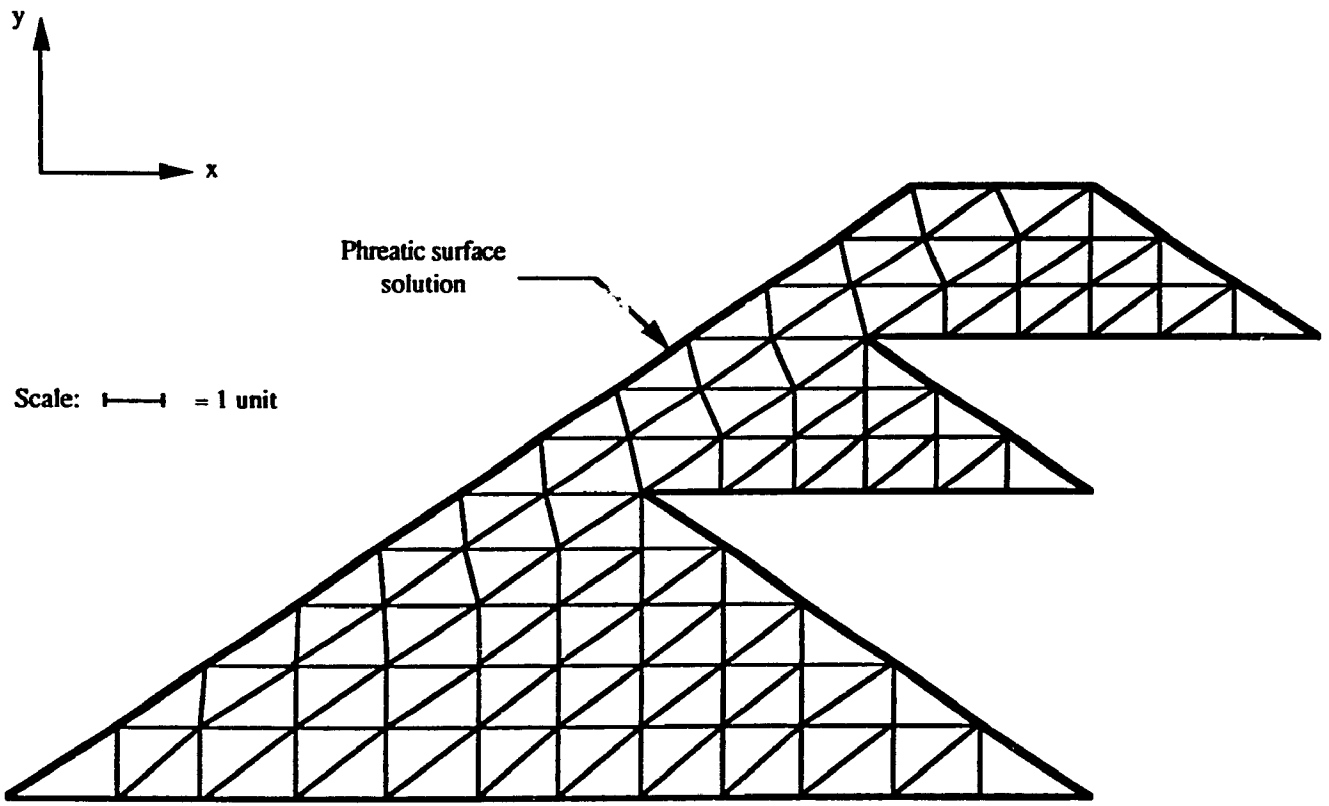

Figure 4.7 Post-Liquefaction Case: Phreatic Surface Solution.

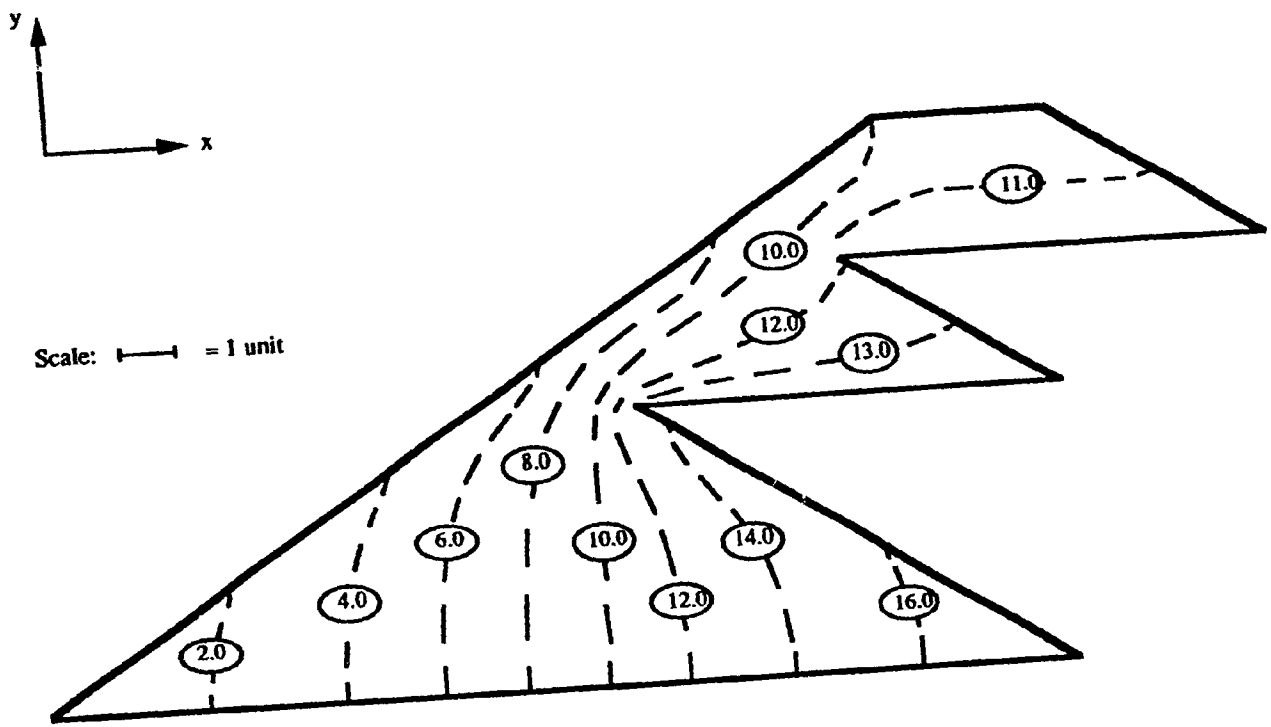

Figure 4.8 Post-Liquefaction Case: Pore Water Pressure Distribution.

CHAPTER 5

COMPARISON AND ANALYSIS OF RESULTS

A qualitative and quantitative comparison of the results obtained for the pre-earthquake and the post-liquefaction cases analyzed in this study will be presented in this chapter. Also, a simple static stability analysis of the tailings dam will be carried out for the post-liquefaction case analyzed, together with discussions on the results obtained.

5.1 Comparison of Results

The phreatic surface solutions for the pre-earthquake case and the post-liquefaction case will be compared qualitatively and quantitatively. Then, a comparison of the pore water pressure at selected points within the body of the tailings dam will be carried out and, a summary of the findings will be presented.

5.1.1 Comparison of Phreatic Surface Solutions

The qualitative comparison of the phreatic surface solutions obtained for the two cases analyzed is easily achieved by referring to the pre-earthquake solution and comparing it to the downstream slope of the tailings dam (refer to Fig. 4.3). This is true for the two cases analyzed in this study because the location of the phreatic surface for the post-liquefaction case coincides with the downstream slope of the tailings dam.

For the quantitative comparison, the difference in the level (i.e., vertical distance) between the phreatic surface solution of the pre-earthquake case and the phreatic surface solution of the post-liquefaction case is obtained. The increase in elevation is measured at selected points located on the phreatic surface solution. In Table 5.1 is presented a summary of the results showing the increase in elevation of the phreatic surface, measured at the four (4) selected points, between the two cases. Refer to Figure 5.1 for the locations

Table 5.1 Increase in Elevation of the Phreatic Surface Solutions at Selected Points

Selected Point	Increase in Elevation (units)
A	1.4
B	2.9
C	2.2
D	1.2

of the selected points on the phreatic surface solution for the pre-earthquake case.

In general, the reults in Table 5.1 indicate that for the selected points, the difference in elevation varies between 1.2 and 2.9 units. As can be seen on Fig. 5.1, smaller differences are obtained for the points selected near the two extremes (i.e., the entrance and exit points), whereas larger differences are obtained for the points selected in between the two extremes. This is due to the shape of the tailings dam, as well as to the fact that the two extremes mentioned above are located at the entrance and exit points of the phreatic surface, into and out of the tailings dam, respectively.

It was claimed by Ishihara (1984) that, prior to the failure of Dam No. 2 of the Mochikoshi tailings impoundment in Japan, the phreatic surface within the tailings dam was located approximately three (3) meters below the downslope face of the dam. However, after liquefaction of the retained material occurred the newly created hydraulic gradient, due to the increase in the pore water pressure, appears to have then raised the elevation of the phreatic surface within the dam. Furthermore, according to his analysis for the movement of the phreatic surface, immediately before failure happened, the phreatic surface was probably very close to the downslope face of the tailings dam.

It is interesting to note that the results obtained for the phreatic surface solution

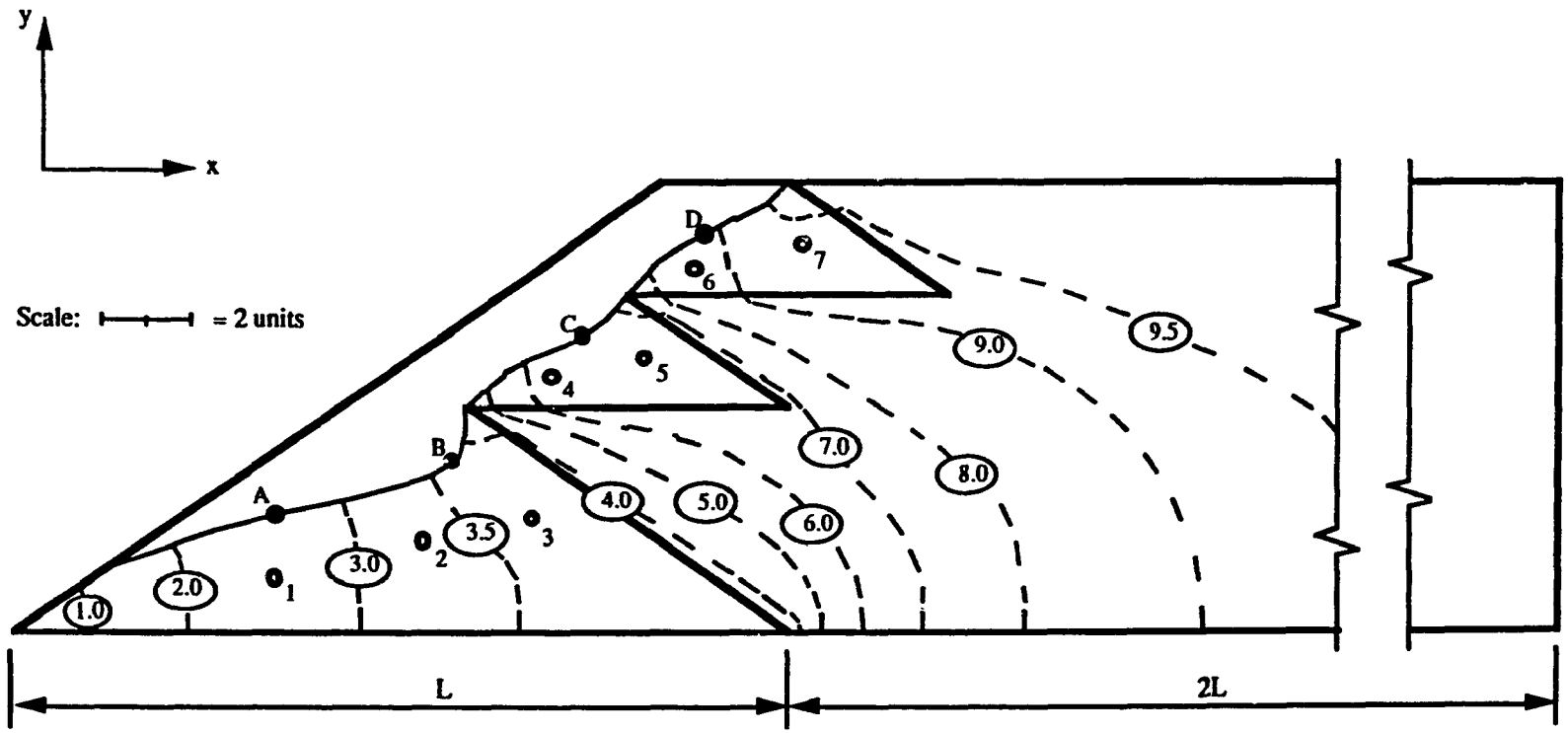

Figure 5.1 Location of Selected Points within the Tailings Dam (Pre-Earthquake Case).

using program PWP for the pre-earthquake case and the post-liquefaction case are similar to those experienced during the sequence of events leading to the Mochikoshi tailings dam failure as described by Ishihara (1984).

5.1.2 Comparison of Pore Water Pressure Distributions

In comparing the pore water pressure distributions within the tailings dam for the two cases analyzed, it is obvious that there is a drastic increase in pore water pressure between the pre-earthquake case and the post-liquefaction case (refer to Figs. 5.1 and 5.2). In the former case, the pore water pressure varies between 0.0 and 10.0 units whereas, for the latter case the pore water pressure varies between 0.0 and 17.6 units.

The pore water pressure in the body of the tailings dam is compared between the two cases analyzed by selecting seven (7) points from within the tailings dam, as shown in Figs. 5.1 and 5.2. For the purpose of obtaining a representative comparison, three (3) of the points are chosen from within the starter dam, whereas two (2) points are chosen from each of the two secondary dams.

In Table 5.2 below, are presented the results of the comparison of the pore water

Table 5.2 Pore Water Pressure (P.W.P.) Increase at Selected Points

Selected Point Number	P.W.P. Pre-EQ.	P.W.P. Post-Liq.	P.W.P. Increase (units)	P.W.P. Increase (%)
1	2.5	5.3	2.8	112.0
2	3.3	9.8	6.5	197.0
3	3.7	13.8	10.1	273.0
4	6.1	12.6	6.5	106.6
5	6.6	12.5	5.9	89.4
6	8.5	11.5	3.0	35.3
7	9.4	11.1	1.7	18.1

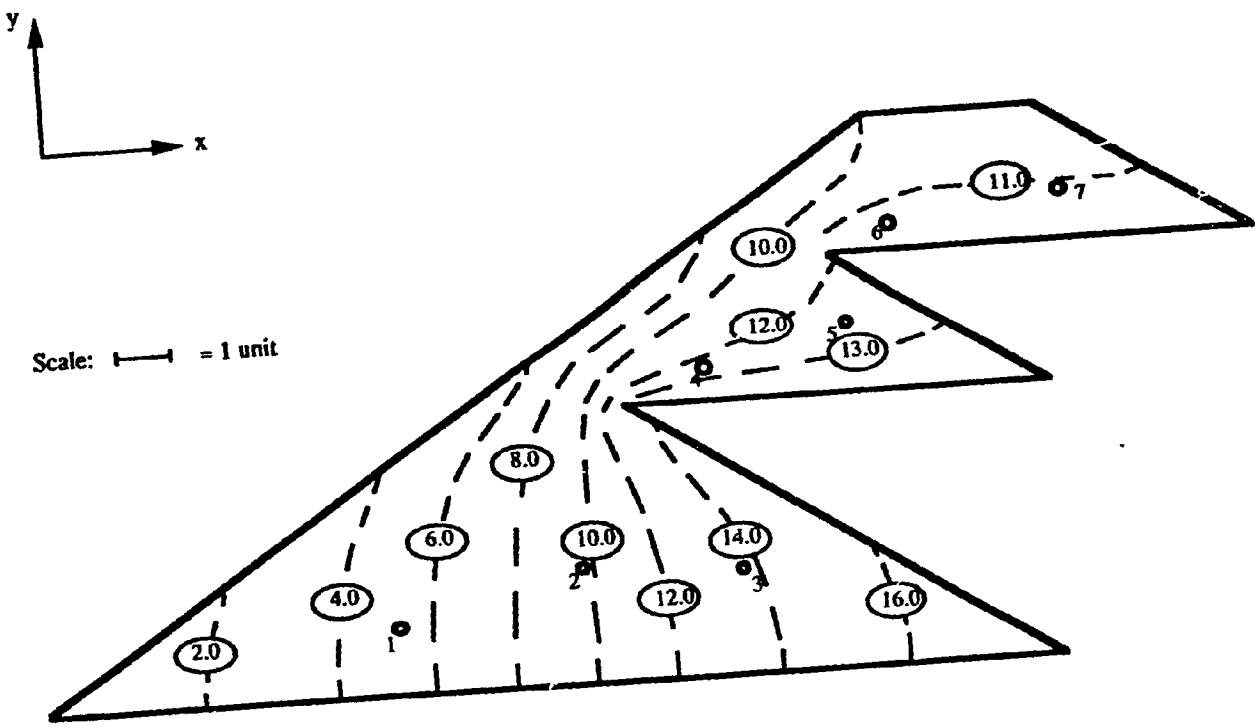

Figure 5.2 Location of Selected Points within the Tailings Dam (Post-Liquefaction Case).

pressure at the seven (7) selected points within the tailings dam. According to the results, the increase in pore water pressure between the two cases varies from 1.7 to 10.1 units and these represent percentage increases varying from 18.1 to 273.0 %, respectively. The largest increases are encountered near the bottom-upstream quadrant of the tailings dam; this is primarily due to the fact that the largest increase in the value(s) of the imposed total head boundary conditions for the post-liquefaction case are situated towards the bottom of the tailings dam's upstream faces.

The results in Table 5.2 are represented graphically on Fig. 5.3 in a bar chart. It is

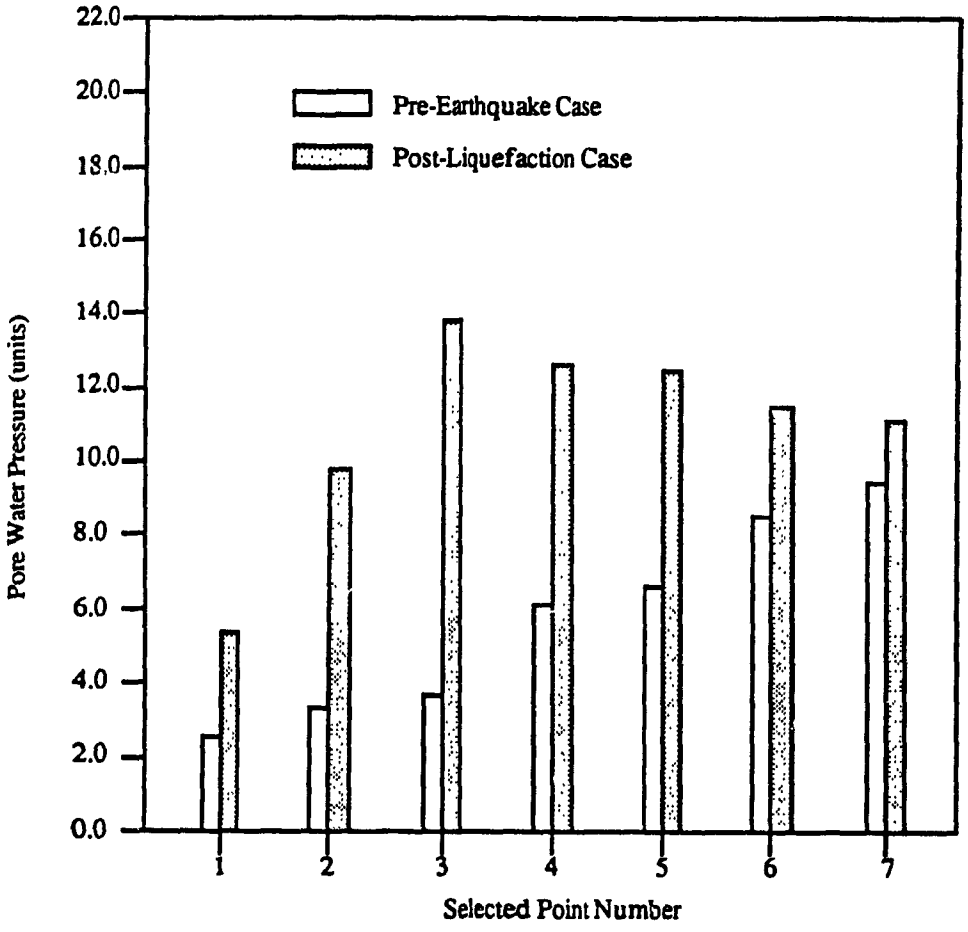

Figure 5.3 Bar Chart Showing the Pore Water Pressure Increase at Selected Points within the Tailings Dam.

quite obvious, graphically from the bar chart, that the results of the pore water pressure for the post-liquefaction case are much higher than those of the pre-earthquake case. Hence, it can be stated that a much higher distribution of pore water pressure is experienced within the tailings dam for the post-liquefaction case and, this is in agreement with the pore water pressure increase that was probably experienced within the Mochikoshi tailings dams prior to their failure (Ishihara, 1984).

5.2 Simple Static Stability Analysis of the Tailings Dam

In order to verify whether the increase in the pore water pressure due to the liquefaction of the retained deposit is sufficient to induce failure of the tailings deposit, a simple static stability analysis of the tailings dam will be performed for the post-liquefaction case. By a simple static analysis, it is understood that a static equilibrium analysis of the external forces acting on judiciously selected portion(s) of the tailings dam will be performed. This method of analysis for the portion of the tailings dam considered will provide a factor of safety regarding the overall stability of the tailings deposit.

For the post-liquefaction case, it is assumed that the material retained behind the tailings dam has completely liquefied, i.e., the pore water pressure, u, increased to the point where it is equal to the total normal stress, σ. Hence, according to equation 2.3, the shear strength, τ, of the liquefied retained material across any plane is equal to zero and therefore, the only shear strength that may be mobilized will have to be from the sand tailings comprising the body of the tailings dam.

The above being the case, we can safely state that the stability of the entire tailings deposit will depend on the shear strength that may be mobilized (i.e., available) along different selected planes within the tailings dam. Effective-stress strength parameters will be used in the stability analysis and therefore, the shear strength that can be mobilized (available) will be a function of the effective normal stress, σ', acting on the selected plane together with the effective-friction angle, ϕ'. The effective-cohesion, c', of tailings will be

taken to be equal to zero because, as mentioned in section 2.1.3, tailings are usually cohesionless and show a zero effective cohesion in laboratory tests.

The most critical plane of failure within the tailings dam (i.e., representing the minimum factor of safety) will be the one for which the ratio between the shear strength that the tailings can mobilize and the applied shear strength is a minimum. From the geometry of the tailings dam, it is obvious that critical planes of failure are located near the boundary where the top of the starter dam coincides with the bottom of the first secondary dam and also, at the boundaries between each pair of adjacent secondary dams where the top of the lower secondary dam coincides with the bottom of the immediate upper secondary dam. This is the case because these critical planes have relatively short lengths and thus, the corresponding shear strength that may be mobilized by the sand tailings along each of these planes will be relatively low.

5.2.1 Method of Simple Static Stability Analysis

In the foregoing analysis, a total of four (4) critical planes are selected within the tailings dam, as shown in Fig. 5.4, and the portions of the tailings dam located above each selected plane is analyzed separately for static stability. That is, the amount of shear strength that may be mobilized by the sand tailings along the selected plane will be compared to the summation of shearing forces acting on the upstream faces of the selected portion of the tailings dam. It should be noted that the shearing forces are caused principally by the component of the effective pressure forces, due to the completely liquefied retained deposit, acting parallel to the selected plane(s).

The method of analysis that will be used shall consist initially of creating a free body diagram showing all the external forces acting upon the portion of the tailings dam located above each of the selected critical planes. The external forces acting on the free body for each selected plane will include the effective weight of the portion of the tailings dam chosen, together with the combined effective weights of slimes bearing upon it and,

the effective pressure forces acting on the upstream faces of the tailings dam and along the selected plane due to the complete liquefaction of the retained deposit. This procedure will permit us to determine the amount of shear strength that may be mobilized as well as the applied shearing forces acting along the chosen plane. Then, the ratio between the applied shearing forces and the shear strength that may be mobilized will provide the factor of safety for the tailings dam along each of the selected planes.

The detailed procedure for the determination of the safety factor for one (1) selected plane within the tailings dam is presented below. The selected plane, identified as line segment A-1 on Fig. 5.4, is the horizontal boundary between the top of the starter dam and the coinciding part of the bottom of the first secondary dam. The free body diagram of the portion of the tailings dam located above plane A-1 together with the external forces acting upon it are shown on Fig. 5.5.

The three (3) types of forces acting on the free body diagram are namely, the effective weights of the material W1, W2 and W3, the effective pressure forces F1, F2, F3, F4 and F5 due to the liquefied retained material, and the shear strength, τ, that may be mobilized along the selected plane A-1

where W1 = effective weight of the entire portion of the tailings dam located above the selected plane

W2 = effective weight of the slimes bearing on the upstream slope of the first secondary dam

W3 = effective weight of the slimes bearing on the upstream slope of the second secondary dam

F1 = effective pressure forces acting along the upstream slope of the first secondary dam

F2 = effective pressure forces acting along the bottom of the first secondary dam

F3 = effective pressure forces acting along the upstream slope of the second secondary dam

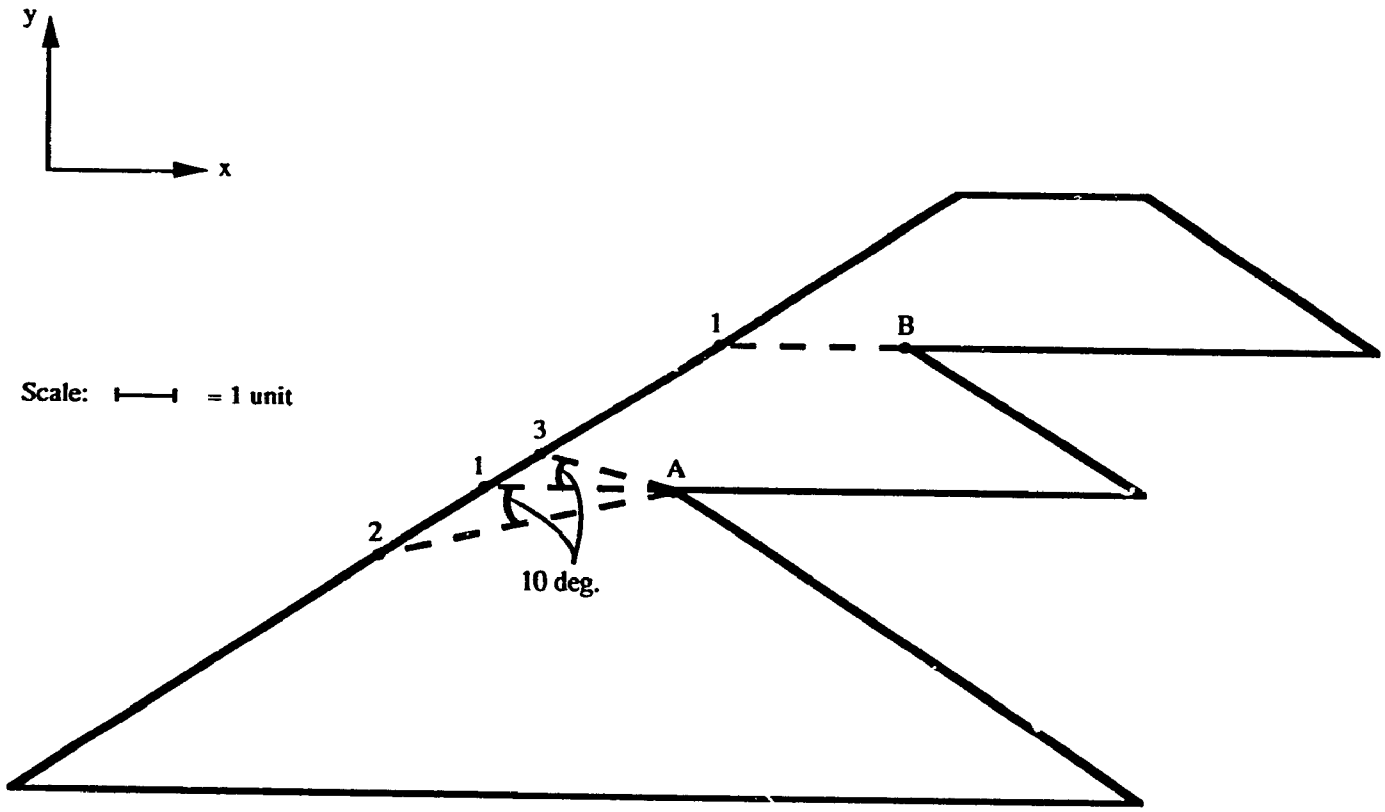

Figure 5.4 Location of Selected Planes within the Tailings Dam (Post-Liquefaction Case).

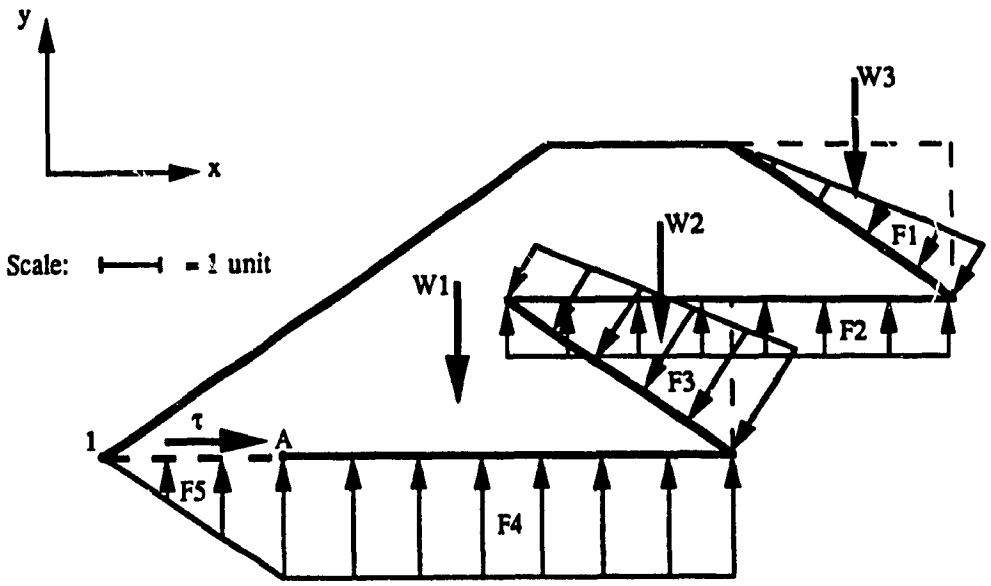

Figure 5.5 Free Body Diagram of Portion of Tailings Dam Above the Selected Plane A-1 showing External Forces.

F4 = effective pressure forces acting along the bottom of the second secondary dam

and F5 = effective pressure forces acting along the selected plane

The first two types of forces namely, the effective weights and the effective pressures may be calculated using, respectively, the material properties and the distribution of effective pressures assumed to be acting on both the upstream faces of the tailings dam and along the selected plane. However, the shear resistance, $\tau = \sigma' \tan \phi'$, acting along plane A-1 may only be calculated after the value of the effective-stress, σ', acting on plane A-1 is determined.

For the selected plane A-1, the values of the effective weights of the materials considered, all acting in the negative y-direction, are the following:

$$W1 = \text{Area} \times \gamma'_{sat\ (sands)} = 2112.8 \text{ lbs}$$

$$W2 = W3 = \text{Area} \times \gamma'_{sat\ (slimes)} = 223.1 \text{ lbs}$$

where, the area of each section is determined from the geometry of the tailings deposit. The effective saturated unit weights for the slimes and the sands are equal to the total unit weight, as determined by equation 4.2, minus the unit weight of water and are approximately 47.6 pcf and 62.6 pcf, respectively. The values of the effective pressure forces, acting perpendicular to each respective face, are:

$$F1 = ((0 + 2.5) / 2) \times 4.51 \times \gamma'_{sat\ (slimes)} = 268.3 \text{ lbs}$$

$$F2 = 2.5 \times 7.5 \times \gamma'_{sat\ (slimes)} = 892.5 \text{ lbs}$$

$$F3 = ((2.5 + 5.0) / 2) \times 4.51 \times \gamma'_{sat\ (slimes)} = 805.0 \text{ lbs}$$

$$F4 = 5.0 \times 7.5 \times \gamma'_{sat\ (slimes)} = 1\ 785.0 \text{ lbs}$$

$$F5 = ((0 + 5.0) / 2) \times 3.0 \times \gamma'_{sat\ (slimes)} = 357.0 \text{ lbs}$$

Next, summation of all the forces acting in the direction perpendicular to the plane of the selected plane is performed and the result is a net force of 419.0 lbs in the negative y-direction. It should be noted that this force is considered to act upon the selected plane A-1 and since the force is acting perpendicular to the selected plane it is taken in its totality, when substituted into equation (2.1), to determine the shear strength which may be mobilized by the sand tailings within the dam.

For the summation of the forces in the direction parallel to the selected plane, the only forces that need to be accounted for are F1 and F3. The value of the summation of these two forces creates the shear force applied on plane A-1 equal to 596.3 lbs, and this value will be used below to determine the factor of safety of the tailings dam for this plane.

The shearing resistance that may be mobilized (i.e., available) along plane A-1 can now be calculated using equation (2.1) as shown:

$$\tau_{available} = \sigma' \tan \phi' = 419.0 \times \tan(35°) = 293.4 \text{ lbs}$$

By comparing the available shearing resistance to the applied shearing force, we obtain the factor of safety (F.S.) of the tailings dam for the selected plane A-1. In this case, we have:

$$F.S. = \tau_{available} / \tau_{applied} = (293.4 \text{ lbs}) / (596.3 \text{ lbs}) = 0.49$$

According to the value of 0.49 for the factor of safety for the stability of the tailings dam obtained from the above static analysis along the selected plane A-1, it is obvious that the tailings dam will fail. To complete our analysis, the factors of safety along the three (3) other selected planes shown in Fig. 5.4 are determined in order to obtain the minimum safety factor (i.e., most critical failure plane) for the tailings deposit.

5.2.2 Results of the Stability Analysis

Proceeding in the same manner as for plane A-1, the factors of safety of the tailings dam for the other three (3) selected planes are determined. The results of the simple static stability analysis carried out for all four (4) selected planes are summarized in Table 5.3. The results indicate that plane A-2 is the most critical failure plane, having the lowest factor of safety of 0.25. It should be noted that this failure plane compares quite closely to the plane of failure measured in the Mochikoshi tailings dams, refer to Fig. 2.8.

However, it must be realized that the factor of safety of 0.25 indicates that the system fails well before the time required for the phreatic surface to coincide with the downstream face of the tailings dam (i.e., post-liquefaction case).

Table 5.3 Safety Factors of Tailings Dam for Selected Planes
(Post-Liquefaction Case)

Selected Plane	Factor of Safety
A-1	0.49
A-2	0.25
A-3	0.63
B-1	2.03

CHAPTER 6

COMMENTS AND CONCLUSIONS

6.1 Findings of this Study

Upon verifying that the computer program PWP, written for this study, provided reliable solutions, the location of the phreatic surface and the corresponding pore water pressure distribution within an upstream construction type of tailings dam were determined for both the pre-earthquake case and the post-liquefaction case.

A quantitative comparison was then performed of the solutions obtained for the two cases analyzed. The results of this comparison show that for the post-liquefaction case, the level of the phreatic surface rose within the tailings dam, and the measured increase in elevation ranged from 1.2 to 2.9 units. The pore water pressure distribution also increased, with the increases ranging between 18.1 and 273.0 %. Furthermore, the location of the phreatic surface is found to coincide exactly with the downstream slope and the top of the dam, indicating that complete saturation of the material comprising the tailings dam occurred.

Using the results obtained for the post-liquefaction case, a simple static stability analysis is carried out. According to this analysis, it is found that the most critical failure plane, identified as line segment A-2, is situated near the top of the starter dam and, has a downward inclination of approximately ten (10) degrees towards the downstream side of the tailings dam. This critical failure plane is shown to compare quite closely to the failure plane of the two Mochikoshi tailings dams that failed in Japan.

Finally, the value of the factor of safety calculated for the most critical failure plane mentioned above is found to be equal to 0.25, indicating that failure of the entire system would easily occur.

6.2 Conclusions

The findings of this research show that the development of the pore water pressure within the retained material creates a hydraulic gradient which causes the phreatic surface to rise within the tailings dam. The rise of the phreatic surface is followed by a corresponding increase of pore water pressure distribution within the tailings dam. Finally, it is shown that this sequence of events leads to a very precarious state of the tailings dam whereby failure of the system is imminent.

Hence, we can conclude that Professor K. Ishihara's diagnosis of the problem, stating that liquefaction of the retained tailings causes the phreatic surface within the tailings dam to rise and subsequently failure of the system to oocur, provides a plausible explanation of the belated-failure phenomenon encountered in tailings deposit.

6.3 Suggestions for Future Work

Future work on tailings dam failures due to liquefaction of the retained deposit may include the densification of the liquefied material. That is, the non-linear properties of tailings and time-dependent variables are considered. In addition, the analysis of different types of tailings dams together with a more rigorous stability analysis of the dam may be carried out during successive stages after the onset of liquefaction in the retained deposit.

REFERENCES

1. Desai, C.S. (1972). "Finite Element Procedure for Seepage Analysis Using an Isoparametric Element," Proceedings of Symposium, Applications of the Finite Element Method in Geotechnical Engineering, U.S. Army Engineer Waterways Experiment Station, Vicksburg, Miss., Vol.2, pp. 799-824.

2. Dobry, R., and Alvarez, L. (1967). "Seismic Failures of Chilean Tailings Dams," Journal of the Soil Mechanics and Foundations Division, ASCE, November.

3. Finn, W.D.L. (1967). "Finite-Element Analysis of Seepage Through Dams," Journal of the Soil Mechanics and Foundations Division, ASCE, November.

4. Finn, W.D.L. (1981). "Seismic Response of Tailings Dams," Proceedings of a Seminar, November 6-7, 1980, Colorado School of Mines, Golden, Colorado, pp. 77-98.

5. Ishihara, K. (1984). "Post-Earthquake Failure of a Tailings Dam Due to Liquefaction of the Pond Deposit," Proceedings of International Conference on Case Histories in Geotechnical Engineering, University of Missouri, Rolla, Mo., Vol. 3, pp. 1129-1143.

6. Jeyapalan, J.K. (1980). "Analyses of Flow Failures of Mine Tailings Impoundments," Ph.D. Dissertation, University of California, Berkeley, August.

7. Klohn, E.J. (1981). "The Development of Current Tailings Dam Design and Construction Methods," Proceedings of a Seminar, November 6-7, 1980, Colorado School of Mines, Golden, Colorado, pp. 1-52.

8. Lucia, P.C., Duncan, J.M. and Seed, H.B. (1980). "Summary of Research on Case Histories of Flow Failures of Mine Tailings Impoundments," U.S. Bureau of Mines Technology Transfer Conference during Spring, 1981, Denver, Colo.

9. Marcuson, W.F., Ballard, R.F. and Ledbetter, R.H. (1979). "Liquefaction Failure of Tailings Dams Resulting from the near Izu Oshima Earthquake, 14 and 15 January 1978," Proceedings of the 6th Panamerican Conference on Soil Mechanics and Foundation Engineering, Lima, Peru, Vol. 2, pp. 69-80.

10. Muskat, M. (1937). The Flow of Homogeneous Fluids Through Porous Media, McGraw-Hill Book Company, New York, N.Y.

11. Okusa S., Anma S. and Maikuma, H. (1980). "Liquefaction of Mine Tailings in the 1978 Izu-Oshima-Kinkai Earthquake, Central Japan," Proceedings of the World Conference on Earthquake Engineering, Englewood Cliffs, N.J., Vol. 3, pp. 89-96.

12. Poorooshasb, H.B. and Ishihara, K. (1989). "Liquefaction Characteristics of Tailings," Proceedings of the International Symposium on Computer and Physical Modelling in Geotechnical Engineering, Rotterdam, Netherlands, pp. 375-381.

13. Verruijt, A. (1982). Groundwater Flow, The Macmillan Press Company, Hong Kong.

14. Vick, S.G. (1983). Planning, Design, and Analysis of Tailings Dams, John Wiley & Sons, New York, N.Y.

15. Weaver Jr., W. and Johnston, P.R. (1984). Finite Elements For Structural Analysis, Prentice-Hall, Englewood Cliffs, New Jersey.

16. Whitman, R.V., Pahwa, A. and Germani, J.T. (1985). "Liquefaction of Soils During Earthquakes," MIT Report, National Academy Press, Washington, D.C.

APPENDIX

```
      PROGRAM PWP
      DIMENSION A(10000)
C
C
C THIS PROGRAM ASSUMES THAT A GIVEN CONTINUUM HAS BEEN DISCRETIZED
C USING CONSTANT HEAD TRIANGLES. ALL SUCH TRIANGLES IN THE
C ANALYTICAL MODEL HAVE THE SAME THICKNESS t, AND THE MATERIAL
C IS TAKEN TO BE LINEARLY ELASTIC, HOMOGENEOUS, AND ISOTROPIC
C (i.e. CONSTANT PERMEABILITY) WITHIN THE DEFINED REGION.
C
C INITIALLY, THE NUMBER OF NODES, NUMBER OF ELEMENTS, NUMBER OF
C DIFFERENT PERMEABILTY, AND THE FIXED HEAD VALUES ARE READ. THIS
C INFORMATION IS THEN PROCESSED ACCORDING TO THE FINITE ELEMENT
C FORMULATION EQUATIONS. FINALLY, THE UNKNOWNS (i.e., PORE WATER
C PRESSURE) FOR THE ORIGINAL SYSTEM OF EQUATIONS ARE SOLVED AND
C PRINTED.
C
C
C     ****************
C     * PROGRAM PWP *
C     ****************
C
C
C-----READ NUMBER OF NODES, NUMBER OF ELEMENTS, AND NUMBER OF
C-----DIFFERENT PERMEABILITY COEFFICIENTS
C
      READ(5,*)NN,NE,NPK
C
C-----CALCULATE POINTERS IN A(XXXXX)
C
      N1=1
      N2=N1+NN
      N3=N2+NN
      N4=N3+NE
      N5=N4+NE
      N6=N5+NE
      N7=N6+NE
      N8=N7+NN
      N9=N8+NN
      N10=N9+NN
      N11=N10+NN
C
C-----CALL SUBROUTINES
C
      CALL SDATA(A(N1),A(N2),A(N3),A(N4),A(N5),A(N6),A(N7),A(N8))
C
      CALL STIFF(A(N1),A(N2),A(N3),A(N4),A(N5),A(N6),A(N8),A(N11))
C
      CALL LDATA(A(N8),A(N9),A(N11))
C
      CALL SKYFAC(A(N8),A(N11))
C
      CALL SKYSOL(A(N8),A(N9),A(N10),A(N11))
C
      CALL RESUL(A(N10))
C
      STOP
      END
```

```
      SUBROUTINE SDATA(X,Y,NMPK,IN,JN,KN,NC,NH)
      COMMON NS,NN,NE,PK(10)
      CHARACTER TITLE*30
      DIMENSION X(1),Y(1),NMPK(1),IN(1),JN(1),KN(1),NC(1),
     1 ID(3),NH(1)
C
C
C SUBPROGRAM SDATA READS AND PRINTS THE PROBLEM IDENTIFICATION,
C STRUCTURAL PARAMETERS, PERMEABILITY COEFFICIENTS, NODAL
C COORDINATES, ELEMENT INFORMATION, AND CALCULATES THE HEAD
C INDICES.
C
C
C     ************************
C     * 1. SUBPROGRAM SDATA *
C     ************************
C
C
C  A) PROBLEM IDENTIFICATION
C
      READ(5,*)TITLE
      WRITE(6,400)TITLE
  400 FORMAT(2X,A30,//)
C
C
C  B) STRUCTURAL PARAMETERS AND PERMEABILITY COEFFICIENTS
C
      WRITE(6,500)
  500 FORMAT(5X,'INITIALIZING DATA')
      WRITE(6,1000)
 1000 FORMAT(4X,'NN',3X,'NE',3X,,'NLS',3X,'NPK')
C
C-----READ AND PRINT INITIALIZING DATA
C
      READ(5,*)NN,NE,NLS,NPK
      WRITE(6,1010)NN,NE,NLS,NPK
 1010 FORMAT(2X,2I5,I4,I6,/)
C
C-----READ AND PRINT DIFFERENT PERMEABILITY COEFFICIENTS
C
      DO 1 I=1,NPK
      READ(5,*)PK(I)
      WRITE(6,1012)I,PK(I)
 1012 FORMAT(1X,'PK(',I2,' ) = ',E12.4,/)
    1 CONTINUE
C
C
C  C) NODAL COORDINATES
C
      WRITE(6,1015)
 1015 FORMAT(1X,'READING COORDINATES OF NODES',/)
      DO 3 K=1,NN
         READ(5,*)J,X(J),Y(J)
    3    CONTINUE
C
C
C  D) ELEMENT INFORMATION
C
      WRITE(6,1035)
 1035 FORMAT(1X,'READING ELEMENT INFORMATION',/)
      DO 4 K=1,NE
C
C--------READ ELEMENT NUMBERS IN CCW DIRECTION
C
         READ(5,*)I,NMPK(I),IN(I),JN(I),KN(I)
```

```
    4     CONTINUE
C
C   E) CALCULATE HEAD INDICES
C
      DO 8 J=1,NN
C
C--------INITIALIZE TERMS IN VECTOR NC TO 1
C
    8     NC(J)=1
      DO 10 I=1,NE
C
C--------CALCULATE THREE HEAD INDICES
C
          ID(1)=IN(I)
          ID(2)=JN(I)
          ID(3)=KN(I)
C
C--------INITIALIZE N1 TO NN
C
          N1=NN
          DO 9 J=1,3
             K=ID(J)
C
C-----------FIND THE MINIMUM HEAD INDEX
C
             IF(K.LT.N1) N1=K
    9        CONTINUE
          DO 10 J=1,3
             K=ID(J)
C
C-----------DETERMINE THE NUMBER OF NON-ZERO TERMS
C
             N2=K-N1+1
C
C-----------UPDATE VECTOR NC
C
             IF(NC(K).LT.N2) NC(K)=N2
   10        CONTINUE
      NH(1)=1
      DO 11 J=2,NN
   11    NH(J)=NH(J-1)+NC(J)
      NS=NH(NN)
      WRITE(6,1060)NS
 1060 FORMAT(1X,'NUMBER OF TERMS IN SN = ',I4,/)
      RETURN
      END
```

```
      SUBROUTINE STIFF(X,Y,NMPK,IN,JN,KN,NH,SN)
      COMMON NS,NN,NE,PK(10)
      DIMENSION X(1),Y(1),NMPK(1),IN(1),JN(1),KN(1),NH(1),
     1 SN(1),SE(3,3),ID(3)
C
C
C THIS SUBPROGRAM NAMED STIFF GENERATES THE 'SKYLINE' IN THE
C UPPER TRIANGLE OF THE NODAL STIFFNESS MATRIX AS A SINGLY
C SUBSCRIPTED VARIABLE BY ASSESSING CONTRIBUTIONS FROM ELEMENT
C STIFFNESSES.
C
C
C     **************************
C     * 2. SUBPROGRAM STIFF *
C     **************************
C
C
C  A) ELEMENT STIFFNESS MATRIX
C
      DO 1 J=1,NS
C
C--------CLEAR NODAL STIFFNESS MATRIX
C
    1    SN(J)=0.0
C
C-----INITIALIZE ELEMENT INDEX TO ZERO
C
      I=0
C
C-----INCREMENT ELEMENT INDEX BY ONE
C
    3 I=I+1
C
C-----CALCULATE DIFFERENCES XIJ, ETC.
C
      XIJ=X(JN(I))-X(IN(I))
      XKI=X(IN(I))-X(KN(I))
      XJK=X(KN(I))-X(JN(I))
      YJI=Y(IN(I))-Y(JN(I))
      YIK=Y(KN(I))-Y(IN(I))
      YKJ=Y(JN(I))-Y(KN(I))
C
C-----CALCULATE AIJK
C
      AIJK=(XIJ*YIK-XKI*YJI)*2
      D=1/(ABS(AIJK))
C
C-----SET APPROPRIATE PERMEABILITY COEFFICIENT NUMBER
C
      NNN=NMPK(I)
C
C-----FILL UPPER TRIANGULAR PART OF SE
C
      SE(1,1)=PK(NNN)*D*((YKJ*YKJ)+(XJK*XJK))
      SE(1,2)=PK(NNN)*D*((YKJ*YIK)+(XJK*XKI))
      SE(1,3)=PK(NNN)*D*((YKJ*YJI)+(XJK*XIJ))
      SE(2,2)=PK(NNN)*D*((YIK*YIK)+(XKI*XKI))
      SE(2,3)=PK(NNN)*D*((YIK*YJI)+(XKI*XIJ))
      SE(3,3)=PK(NNN)*D*((YJI*YJI)+(XIJ*XIJ))
C
C
C  B) TRANSFER TO SYSTEM STIFFNESS MATRIX
C
C
C-----SET HEAD INDICES IN GENERAL
```

```
C
      ID(1)=IN(I)
      ID(2)=JN(I)
      ID(3)=KN(I)
      DO 5 J=1,3
         DO 5 K=J,3
C
C-----------SET ROW INDEX
C
            IR=ID(J)
C
C-----------SET COLUMN INDEX
C
            IC=ID(K)
C
C-----------CHECK WHETHER ROW INDEX IS LESS OR EQUAL TO
C-----------COLUMN INDEX
C
            IF(IR.LE.IC) GOTO 4
C
C-----------IF NOT,INTERCHANGE ROW AND COLUMN INDICES
C
            ITEM=IR
            IR=IC
            IC=ITEM
C
C-----------CALCULATE INDEX IN MATRIX SN
C
4           IRC=NH(IC)-(IC-IR)
C
C-----------TRANSFER A TERM IN SE TO SN
C
            SN(IRC)=SN(IRC)+SE(J,K)
5           CONTINUE
      IF(I.LT.NE) GOTO 3
      RETURN
      END
```

```
      SUBROUTINE LDATA(NH,AN,SN)
      COMMON NS,NN
      DIMENSION NH(1),AN(1),SN(1)
C
C
C SUBPROGRAM LDATA READS, PRINTS AND PROCESSES THE LOAD DATA
C
C
C     ************************
C     * 3. SUBPROGRAM LDATA  =
C     ************************
C
C
C  A) HEAD PARAMETERS
C
C-----READ AND PRINT NUMBER OF FIXED HEADS
C
      READ(5,*)NFH
      WRITE(6,2000)NFH
 2000 FORMAT(1X,'NUMBER OF FIXED HEADS = ',I3,/)
C
C-----CLEAR NODAL HEAD VECTOR
C
      DO 13 J=1,NN
   13    AN(J)=0.0
C
      WRITE(6,2020)
 2020 FORMAT(1X,'READING FIXED HEAD VALUES',/)
      DO 16 JJ=1,NFH
C
C--------READ FIXED HEAD VALUES
C
         READ(5,*)II,VALUE
C
C--------MAGNIFY VALUES OF SN(II) AND AN(II)
C
         SN(NH(II))=1.0E8
         AN(II)=SN(NH(II))*VALUE
   16    CONTINUE
      RETURN
      END
```

```
      SUBROUTINE SKYFAC(NH,A)
      COMMON NS,NH,NE
      DIMENSION NH(1),A(1)
C
C
C     *************************
C     * 4. SUBPROGRAM SKYFAC *
C     *************************
C
C
C IN SUBPROGRAM SKYFAC, A 'SKYLINE' PATTERN OF NONZERO TERMS
C APPEARS IN THE UPPER TRIANGLE OF THE SYMMETRIC MATRIX A( , ).
C THE SAME INFORMATION IS STORED MORE COMPACTLY AS A VECTOR
C A( ). FINALLY, THE MATRIX 'U' IS GENERATED AND PLACED IN THE
C STORAGE LOCATIONS ORIGINALLY OCCUPIED BY THE MATRIX 'A'.
C
C
      N=NN
      IF (A(1).LE.0.0) RETURN
      DO 7 J=2,N
C
C--------OBTAIN POINTER AND DIAGNOL POSITION FOR COLUMN J.
C--------ALSO CALCULATE NCJ.
C
         J1=J-1
         NJ=NH(J1)
         JJ=NH(J)
         NCJ=JJ-NJ
         IF (NCJ.EQ.1) GOTO 7
         IF (J1.EQ.1) GOTO 5
         DO 4 I=2,J1
C
C-----------FIND J MINUS I
C
            JMI=J-I
C
C-----------CHECK WHETHER COLUMNS I AND J INTERACT
C
            IF (NCJ.LE.(JMI+1)) GOTO 4
C
C-----------IF SO, FIND THE INDICES SHOWN
C
            I1=I-1
            NI=NH(I1)
            NJ=NH(J1)
            II=NH(I)
            IJ=NJ-JMI
            NCI=II-NI
            NCJI=NCJ-JMI
            NCD=NCJI-NCI
C
            IF (NCD.GE.0) THEN
C
C-----------IF NCD +VE, SET K1 AND SHIFT POINTER FOR COLUMN J
C
            K1=NCI-1
            NJ=NJ+NCD
            ELSE
C
C-----------IF NCD -VE, SET K1 AND SHIFT POINTER FOR COLUMN I
C
            K1=NCJI-1
            NI=NI-NCD
            ENDIF
            SUM=A(IJ)
```

```
            IF (K1.EQ.0) GOTO 4
            DO 3 K=1,K1
C
C--------------LOCATE A(KI) AND A(KJ)
C
               KI=NI+K
               KJ=NJ+K
C
               IF (ABS(A(KJ)).LT.1.E-10) A(KJ)=0.
               SUM=SUM-A(KI)*A(KJ)
    3          CONTINUE
            A(IJ)=SUM
    4       CONTINUE
    5     SUM=A(JJ)
          NCJ1=NCJ-1
C
            DO 6 K=1,NCJ1
C
C-----------LOCATE A(KJ) AND A(KK) AND DIVIDE.
C
            KJ=NN(J1)+K
            KK=NN(J-NCJ+K)
            TEMP=A(KJ)/A(KK)
            SUM=SUM-TEMP*A(KJ)
C
            A(KJ)=TEMP
    6       CONTINUE
          IF(SUM.LE.0.0) RETURN
          A(JJ)=SUM
    7     CONTINUE
        RETURN
        END
```

```
      SUBROUTINE SKYSOL(NH,B,X,U)
      COMMON NS,NN,NE
      DIMENSION NH(1),B(1),X(1),U(1)
C
C
C     *************************
C     * 5. SUBPROGRAM SKYSOL *
C     *************************
C
C
C THIS SUBPROGRAM, SKYSOL, ACCEPTS THE FACTOR 'U' FROM SUBROUTINE
C SKYFAC AND SOLVES FOR THE UNKNOWNS IN THE ORIGINAL SYSTEM OF
C EQUATIONS.
C
C
         N=NN
      DO 2 I=1,N
         SUM=B(I)
         IF (I.EQ.1) GOTO 2
C
C--------OBTAIN POINTER AND DIAGONAL POSITION FOR COLUMN I.
C--------THEN FIND NCI,K1,AND R.H.S. POINTER KR.
C
         I1=I-1
         NI=NH(I1)
         II=NH(I)
         NCI=II-NI
         K1=NCI-1
         KR=I-NCI
         IF (K1.EQ.0) GOTO 2
         DO 1 K=1,K1
C
C-----------LOCATE U(K1) AND R.H.S. TERM
C
            KI=NI+K
            KR=KR+1
            SUM=SUM-U(KI)*X(KR)
    1       CONTINUE
    2    X(I)=SUM
      DO 3 I=1,N
C
C--------LOCATE U(II)
C
         II=NH(I)
         X(I)=X(I)/U(II)
    3    CONTINUE
      DO 5 I1=1,N
         I=N-I1+1
         K2=I+1
         SUM=X(I)
         IF (I.EQ.N) GOTO 5
         DO 4 K=K2,N
C
C-----------CALCULATE THE INDICES SHOWN
C
            K1=K-1
            KMI=K-I
            NK=NH(K1)
            NCK=NH(K)-NK
            NCKI=NCK-KMI
C
C-----------CHECK WHETHER U(IK) EXISTS
C
            IF (NCKI.LE.0) GOTO 4
C
```

```
C-----------IF SO, LOCATE U(IK)
C
              IK=NK+NCKI
              SUM=SUM-U(IK)*X(K)
    4         CONTINUE
    5       X(I)=SUM
          RETURN
          END
```

```
      SUBROUTINE RESUL(HN)
      COMMON NS,NN,NE
      DIMENSION HN(1)
C
C
C THE FINAL OUTPUT OBTAINED FROM THE SUBPROGRAM RESUL IS THE
C CALCULATED HEAD VALUES FOR EACH NODE.
C
C
C     ************************
C     * 6. SUBPROGRAM RESUL *
C     ************************
C
C
      WRITE(6,2042)
 2042 FORMAT(1X,'CALCULATED HEAD VALUES AT NODES',/)
      WRITE(6,2045)
 2045 FORMAT(5X,'NODE    HEAD VALUE',/)
C
      DO 1 J=1,NN
C
C--------PRINT NODES AND HEAD VALUES
C
    1    WRITE(6,2050)J,HN(J)
 2050    FORMAT(4X,I4,F12.5)
      RETURN
      END
```